SELENOLOGY TODAY

Geological Lunar Researches Group

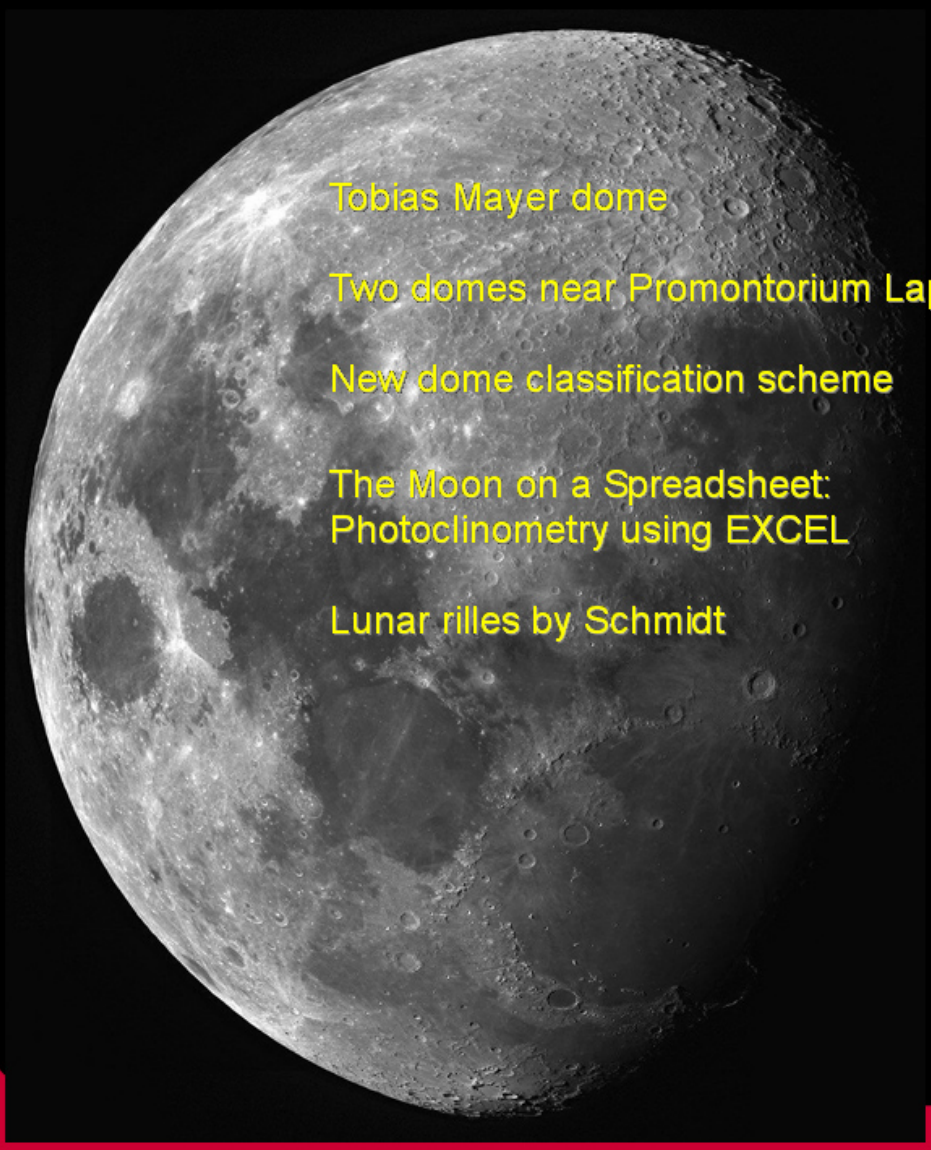

Tobias Mayer dome

Two domes near Promontorium Laplace

New dome classification scheme

The Moon on a Spreadsheet:
Photoclinometry using EXCEL

Lunar rilles by Schmidt

Selenology Today #1 June 2006

Selenology Today is devoted to the publication of contributions in the field of lunar studies.

Manuscripts reporting the results of new research concerning the astronomy, geology, physics, chemistry and other scientific aspects of Earth's Moon are welcome.

Selenology Today publishes papers devoted exclusively to the Moon.

Reviews, historical papers and manuscripts describing observing or spacecraft instrumentation are considered.

The Selenology Today

Editorial Office

selenology_today@christian-woehler.de

SELENOLOGY TODAY #1
June 2006

Geological Lunar Researches Group

Cover : Giorgio Mengoli, image taken on November 11, 2005. Refractor ED80mm feq.600mm . Camera CCD DMK (15fps), filter IRcut. 190 frames Registax, AstroArt3, Psp8

Welcome to the first issue of Selenology Today.

Selenology Today is a new online journal devoted to studies of the Moon, mainly of observational, geological, and historical nature. It will appear twice per year.

Despite the fact that the Moon has been visited by six manned missions and a multitude of unmanned spacecraft, its surface is far from being completely explored. After the last manned mission, Apollo 17, which took place in 1972, it was not before 1994 that the Moon was visited by a spacecraft again: Clementine performed a nearly complete multispectral mapping with state-of-the-art imaging sensors in the visible, near and mid infrared wavelength range. The Clementine mission as well as the Lunar Prospector spacecraft launched in 1998 have stimulated a broad range of scientific activities dealing with the geology and surface composition of the lunar surface. The Clementine image data, however, are largely unsuitable for photogeologic and topographic analyses due to the low phase angles and high illumination angles at which most of them were acquired. Hence, the best available set of spacecraft images globally covering the lunar surface, taken under low to moderate illumination angles and thus revealing the relief of the lunar surface, is still that obtained during the Lunar Orbiter programme in the mid-1960s. The ongoing Smart 1 mission, which is intended to be terminated by a spectacular crash of the spacecraft on the lunar surface at the end of September 2006, will provide the first high-resolution set of orbital lunar images acquired with modern sensory devices primarily at oblique illumination.

As a consequence of the fact that during the last three decades the Moon has merely been the target of three spacecraft missions with rather specialised scientific goals, respectively, many questions still remain open. What is more, our neighbour in space is one of the few solar system bodies for which images and spectra taken with state-of-the-art ground-based instrumentation and even amateur equipment may be of high scientific value and provide novel insights into the geology and topography of regions of the lunar surface.

Hence, the primary goal of Selenology Today is to promote serious lunar research among dedicated amateur astronomers who are interested in observing and imaging the surface of the Moon as well as in its geologic history and the processes that formed its surface. We will also attempt to attract as an audience professional planetary scientists with a special interest in lunar research.

Selenology Today is published by the Geologic Lunar Research (GLR) group. Founded in 1997, the GLR group is an informal international association of dedicated lunar observers sharing a common interest in all domains of lunar science, especially in the field of lunar volcanism. While many GLR members are specialised in high-resolution CCD imaging of the lunar surface, in particular lunar domes, some concentrate on the evaluation of the obtained imagery with respect to the morphologic or topographic features of the imaged surface regions, and others are interested in transient lunar phenomena (TLP) and the critical assessment of the corresponding observations. Relevant results of GLR projects are published in scientific journals as combined efforts by the group members.

This first issue of Selenology Today is composed of several sections. The Domes section features two articles describing the observation of three previously unknown, newly discovered lunar domes and implications about their morphometric and rheologic properties. A further article summarises a novel classification scheme for lunar mare domes which is based on their spectral and morphometric characteristics. This classification approach is the result of a combined work by several GLR members and has been published in an extensive article currently in press at the journal Icarus. The section Geological Lunar Research is made up of contributions to different aspects of lunar science. The articles in this section have been peer-reviewed by members of the editorial board. In the current issue, this section features an article about an efficient and easy-to-use approach to image-based three-dimensional reconstruction of regions of the lunar surface. The Historical Note section contains articles of historical interest, focusing here on drawings of lunar rilles performed in the middle of the 19th century by the German selenologist Julius Schmidt.

The articles in this first issue of Selenology Today were all written by GLR members. However, a broad basis of contributors is needed to ensure on the long term a good quality of the journal. Hence, we strongly encourage all readers of Selenology Today to submit articles describing the results of their own lunar research.

And now I hope you will enjoy reading the first issue of Selenology Today !

Raffaello Lena
Editor in Chief

The Hortensius-Milichius-Tobias Mayer region: An unlisted dome located at 25.17° W and 6.07° N

by Raffaello Lena, Christian Wöhler, Jim Phillips, and Maria Teresa Bregante
Geologic Lunar Research (GLR) group

Abstract

In this study we describe a previously unreported dome, here named Hortensius 24, at selenographic coordinates 25.17° W and 6.07° N. It is 21 km in diameter, 110 m high, with an average flank slope of 0.6°, and has a summit fissure. Hortensius 24 is a C_1 dome in the GLR classification scheme. Rheologic modelling of the dome suggests that the dome was built by lava of low viscosity, erupted at a high effusion rate over nine months.

1. Introduction

Lunar domes are gentle swells, a few hundred metres high, similar to low shield volcanoes found on Earth. They represent the terminal phase of a lunar eruption and they occur mostly in the maria.

Fig.1: Jim Phillips on February 08, 2006, at 02:24 UT.

The geologic processes involved in lunar volcanism were examined in the context of the Basaltic Volcanism Study Project (1981) and are also discussed in detail e. g. by Head and Gifford (1980). According to these descriptions, constructional volcanic features formed during the later stages of volcanism on the Moon, characterised by a decreasing rate of lava extrusion and comparably low temperature of eruption, resulting in the formation of effusive domes.

A few domes have been reported in the highlands, but are usually difficult to see because of the brightness and ruggedness of the region (Lena et al. (2003) and references therein). The region west of Copernicus extending from Hortensius to Milichius and on to Tobias Mayer contains

large numbers of lunar domes and cones, evidence of past volcanism on the lunar surface. Schroeter (1791, 1802) was the first to record a lunar dome. He included drawings of the dome near Milichius in his work *Selenotopographische Fragmente*. Goodacre (1930) in his classic book *The Moon* includes a drawing of the six domes north of Hortensius by Schlumberger dated April 08, 1930. Continued efforts at mapping this region ensued over the remainder of the 20th century. A comprehensive map of the area was produced by Phillips (1989). The map was the result of a detailed investigation using several sources such as ALPO observers, *The Times Atlas of the Moon* (Lewis, 1969), the *New Photographic Atlas of the Moon* by Kopal et al. (1965), the Copernicus Quadrangle of the Moon (LAC 58), the Kepler Quadrangle of the Moon (LAC 57), and the photographic lunar atlas by Kuiper et al. (1967). This region was also extensively studied by Head and Gifford (1980) showing that domes of different shapes and slopes occur together.

In this study we describe a previously unreported dome at 25.17° W and 6.07° N, named Hortenius 24, according to the revised catalogue of lunar domes recently published by Kapral and Garfinkle (2005).

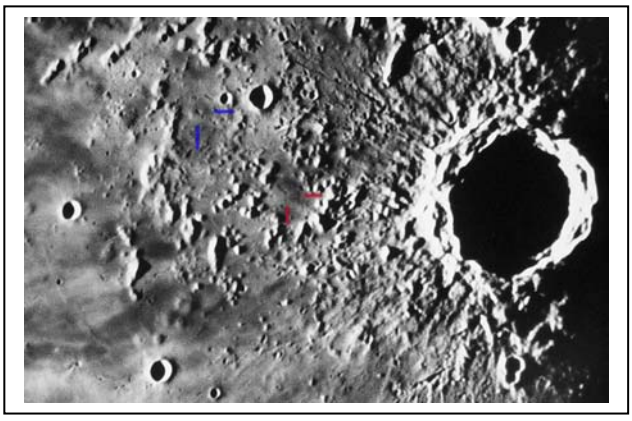

Fig.2: Consolidated Lunar Atlas D 23. The dome Examined here, located at longitude 25.17°W and Latidude 6.07°N, is marked in red, while a well known Dome located near Tobia Mayer D at longitude 27.30°W And latitude 11.95°N is marked in blue.

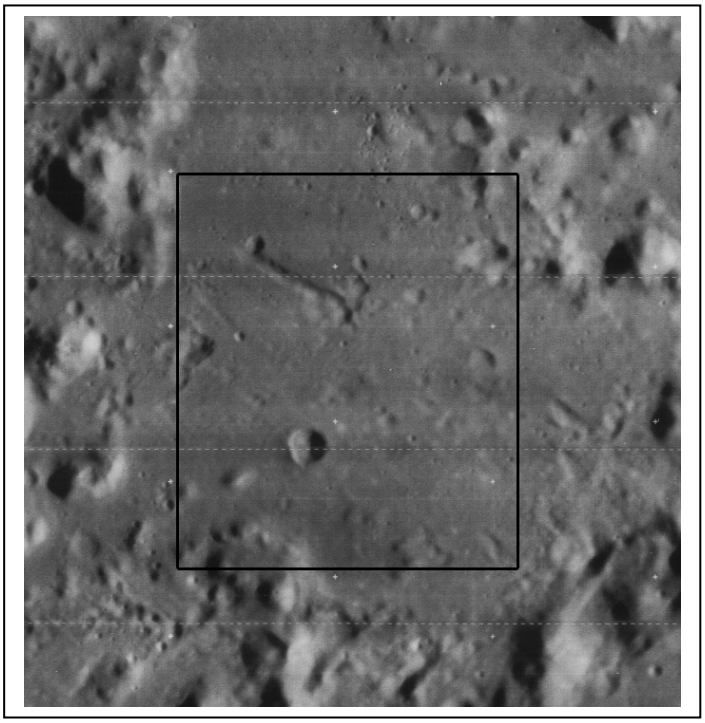

Fig.3: Lunar Orbiter frame IV-133-H2.

2. Observations

A shallow dome has been observed near the crater Tobias Mayer C, and is described here. The dome is located at 25.17° W and 6.07° N (Xi = −0.423, Eta = +0.106). It is, to our knowledge, previously unreported in any lunar dome survey. For each of the observations, the local solar altitude and the Sun's selenographic colongitude were calculated using the Lunar Observer's Toolkit by H. D. Jamieson. All the images are oriented with north up and west (IAU) to the left.

The dome was detected on an image (Fig. 1) taken by Jim Phillips on February 08, 2006, at 02:24 UT using a 200 mm TMB apochromatic refractor, and an Atik B&W camera (solar altitude = 2.06°, colongitude = 27.36°). The scale of the image is 0.29 km per pixel. In Fig. 1, the shading on the dome's antisolar flank is not black, indicating that the slope is of low inclination. Preliminary estimations indicate a diameter of about 21 km and a rather low slope; the outline of the dome is not well-defined. Furthermore, a summit fissure, with an estimated size of 3.9 ± 0.30 km, is apparent. Fig. 2 shows an image from the *Consolidated Lunar Atlas*, D23, where the low dome is detectable, with the elongated fissure visible on the summit. The dome described here is marked in red, while a well known dome located near Tobias Mayer D at longitude 27.38° W and latitude 11.95° N is marked in blue. Fig. 3 displays Lunar Orbiter frame IV-133-H2, where the elongated fissure is also recognisable. In this image, the fissure appears rimless and without a sharp outline, which supports our interpretation that it is of volcanic origin. Its rim does not cast a black shadow. In contrast, impact craters in Figure 3 appear to be significantly deeper than the fissure since they are filled with black shadows.

Table 1: Properties of the dome located at 25.17° W and 6.07° N, measured in Fig.1

Dome	Longitude Latitude	Diameter [km]	Height [m]	Slope [°]	Volume [km^3]
Dome 1	-25.17° +6.07°	21	110 ± 10	0.60 ± 0.1	16.6 ± 3.3

Table 2: Approximate spectral and morphometric properties characterising the dome classes described by Wöhler et al (2006).

Class	TiO_2 content	Slope [°]	D [km]	V [km^3]
A	high	0.3-1.0	5-13	<3
B_1	moderate	2.0-5.4	6-15	5-32
B_2	moderate	1.3-1.9	8-15	2-21
C_1	low to moderate	0.6-1.8	13-20	7-33
C_2	moderate to high	1.0-2.5	8-17	4-17
D	high	1.3-2.5	≈25	40-67

3. Morphologic, morphometric, and spectral properties

According to the empirical relation between vent diameter and dome base diameter established by Head and Gifford (1980) for effusive mare domes, the expected value for the vent diameter is 3.9 km, given the dome diameter of D = 21 km, which is in very good agreement with our measured value.
Further morphometric data were obtained by generating a 3D profile of the dome from the image shown in Fig. 1, relying on a photoclinometric analysis (Horn, 1989; Wöhler et al., 2006; Lena et al., 2006, and references therein). The result is shown in Fig. 4 as a cross section through the dome summit in east-west direction (red curve). The effective height of the dome was obtained by determining elevation differences between the summit of the dome and its surroundings, taking into account the curvature of the lunar surface (blue curve). This leads to a dome height of 110 ± 10 m, yielding an average flank slope of 0.6° ± 0.1°.
The dome edifice volume was determined by computing the volume of the body generated by rotating the cross-section shown in Fig. 4 around a vertical axis through the summit, resulting in a volume of 16.6 km³.
A rough quantitative measure for the shape of the dome is given by the form factor:
$f = V/[\pi h(D/2)^2]$, where we have $f = 1/3$ for domes of conical shape, $f = 1/2$ for parabolic shape, $f = 1$ for cylindrical shape, and intermediate values for hemispherical shape (Wöhler et al., 2006). For the dome examined in this study, we obtain $f = 0.44$.
The Clementine UVVIS spectral data of the dome reveal for the dome near Tobias Mayer C a rather high 750 nm reflectance of $R_{750} = 0.1411$, a moderate value for the UV/VIS colour ratio of $R_{415}/R_{750} = 0.5920$, indicating a moderate TiO_2 content, and a weak mafic absorption with $R_{950}/R_{750} = 1.0389$, indicating a high soil maturity.

4. Rheologic modelling

We assume that the examined dome was formed by extrusion of magma onto a flat plane spreading in all directions from the vent, in contrast to lava flows resulting from lava extrusion onto an inclined surface. Wilson and Head (2003) provide a quantitative treatment of such dome-forming eruptions. This model estimates the yield strength τ, i. e. the pressure or stress that must be exceeded for the lava to flow, the plastic viscosity η, yielding a measure for the fluidity of the erupted lava, the effusion rate E, i. e. the lava volume erupted per second, and the duration T = V/E of the effusion process. This model is applied to a large set of representative lunar mare domes by Wöhler et al. (2006). It relies on the morphometric dome properties (diameter, height, volume) and several physical constants such as the lava density, the acceleration due to gravity, and the thermal diffusivity of the lava. The computed values for η, τ, E, and T obtained with the model by Wilson and Head (2003) are valid for domes that

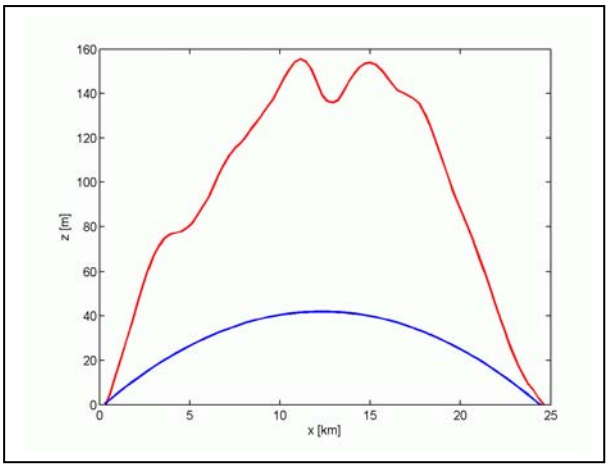

Fig.4: Cross-section through the dome examined Summit (red), curved lunar reference surface (blue)

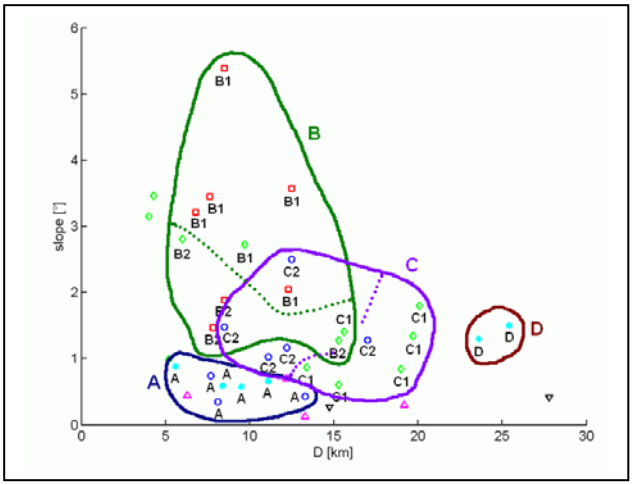

Fig.5: Diameter vs. flank slope a set of 38 lunar mare domes, after Wöhler et al. (2006). The domes are labelled accordingto their respective class as defined in Table 2.

formed from a single flow unit (monogenetic volcanoes). Otherwise, the computed rheologic values are upper limits to the respective true values.
The low slope and large diameter of the dome regarded in this study suggest a high effusion rate, a low lava viscosity, and a short duration of the effusion process. The rheologic model by Wilson and Head (2003) yields an effusion rate of 704 m^3/s. The dome formed out of lava with a viscosity of 1.5 x 10^4 Pa s over a period of time of 0.9 years.

5. Results and discussion

Many lunar domes have a summit crater pit likely representing the vent of the volcano which was enlarged by magma withdrawal and/or later erosion. The dome examined here does not display a circular summit pit but its summit is crossed by a rimless elongated fissure of 3.9 km length (see Fig. 3). Volcanoes can have such elongated vents especially when they were formed along a fissure or by a dike intrusion. Hence, this depression represents the original vent, the place at which lava poured out over the lunar surface, successively building up a shield-like volcano around it. Another, previously known dome to the north-west (Fig. 2) also exhibits a summit with an elongated fissure.
Wöhler et al. (2006) examined the spectral properties and 3D shapes of a set of 38 effusive lunar mare domes, and developed a classification scheme. According to this new GLR dome classification scheme,

Hortensius 24 is a C_1 dome. As a general trend, shallow and steep domes formed out of low or moderate TiO_2 basalts are observed in the Hortensius and Milichius dome fields. In this scheme, class C_1 includes mare domes characterised by moderately red lavas in terms of Clementine UV/VIS colour ratio, a moderate TiO_2 content and a flat, pancake-shaped appearance with shallow slopes of less than 2°, implying low lava viscosities and high effusion rates. For comparison, in the diameter vs. flank slope diagram shown in Fig. 5 the domes of the set examined by Wöhler et al. (2006) are labelled according to their respective classes as defined in Table 2.

Future work will include an extension of our analysis to other effusive mare domes in the Hortensius/ Milichius/Tobias Mayer region. Such analyses will provide insight into the global and regional internal geologic processes responsible for the formation of the observed various types of lunar domes in this complex volcanic region.

References

[1] Basaltic Volcanism Study Project. *Basaltic Volcanism on the Terrestrial Planets*. Pergamon Press, Inc., New York, 1981.

[2] Goodacre W., *The Moon*, 1930.

[3] Head J. W., Gifford A., Lunar mare domes: classification and modes of origin, *The Moon and Planets* 22, 235-257, 1980.

[4] Horn B. K. P., Height and Gradient from Shading, MIT technical report, AI memo no. 1105A, 1989. http://people.csail.mit.edu/people/bkph/AIM/AIM-1105A-TEX.pdf

[5] Kapral, C., Garfinkle, R., 2005. GLR Lunar Dome catalog. http://www.glrgroup.org/domes/kapralcatalog.htm

[6] Kopal Z., Klepešta J., Rackman T., Thomas W., *Photographic Atlas of the Moon*, Academic Press, 1965.

[7] Lewis H. A. G. (ed.), *The Times Atlas of the Moon*, Times, London, 1969.

[8] Lena R., Viegas R., Fattinnanzi C., A study about Highland domes: a generic classification of the dome near Piccolomini, located at 28.69° E and 27.50° S, JALPO, 45(3), 22-27, 2003 .

[9] Lena R., Wöhler C., Bregante M. T., Fattinnanzi C, A combined morphometric and spectrophotometric study of the complex lunar volcanic region in the south of Petavius, *JRASC* 100(1), 14-25, 2006.

[10] Phillips J., The New Lunar Dome Survey: the Hortensius-Milichius-Tobias Mayer Region, *JALPO* 33(4-6), 61-72, 1989.

[11] Schroeter J., *Selenotopographische Fragmente*, 1791, 1802.

[12] Wilson L., Head J. W., Lunar Gruithuisen and Mairan domes: Rheology and mode of emplacement, *J. Geophys. Res*. 108(E2), 5012-5018, 2003.

[13] Wöhler C., Lena R., Lazzarotti P., Phillips J., Wirths M., Pujic Z., A combined spectrophotometric and morphometric study of the lunar mare dome fields near Cauchy, Arago, Hortensius, and Milichius, *Icarus*, in press, 2006.

A STUDY ABOUT TWO UNLISTED DOMES NEAR PROMONTORIUM LAPLACE

by Raffaello Lena, Christian Wöhler, Alexander Wöhler, Jim Phillips, KC Pau, Paolo Lazzarotti and Maria Teresa Bregante
Geologic Lunar Research (GLR) group

Abstract

Morphometric details were established for two previously unlisted domes in eastern Sinus Iridum. The first, named Laplace 5, is located at longitude 28.66° W and latitude 47.17° N, and has a diameter of 9.0 ± 0.5 km. Based on four independently acquired CCD images, its height was determined to 128 m with an average slope of 1.6°. The second dome, here named Laplace 6, is situated at longitude 29.16° W and latitude 47.08° N and has a diameter of 15 km, a height of 95 m and an average slope of 0.7°. Laplace 5 is a B_2 dome in the GLR classification scheme, while Laplace 6 is probably a dome of intrusive nature. Rheologic modelling of the effusive dome Laplace 5 suggests that it was built by lava of moderate viscosity, erupting at a high effusion rate over a period of time of 1 year.

1.Introduction

Sinus Iridum is a plain of basaltic lava that forms a northwestern extension to Mare Imbrium. It is surrounded from the northeast to the southwest by the Montes Jura. The protruding southwestern end is named Promontorium Heraclides, while the northeastern rim is called Promontorium Laplace. Different lithological units, included in USGS lunar geologic map I-602, are apparent in the Sinus Iridum region mapped as 3 distinct units, Im1 through Im3, and described as flat, smooth material of mare areas (Schaber, 1969).

Sinus Iridum does not contain any important impact craters, except the crater Heraclides E in the south and the crater Laplace A at the

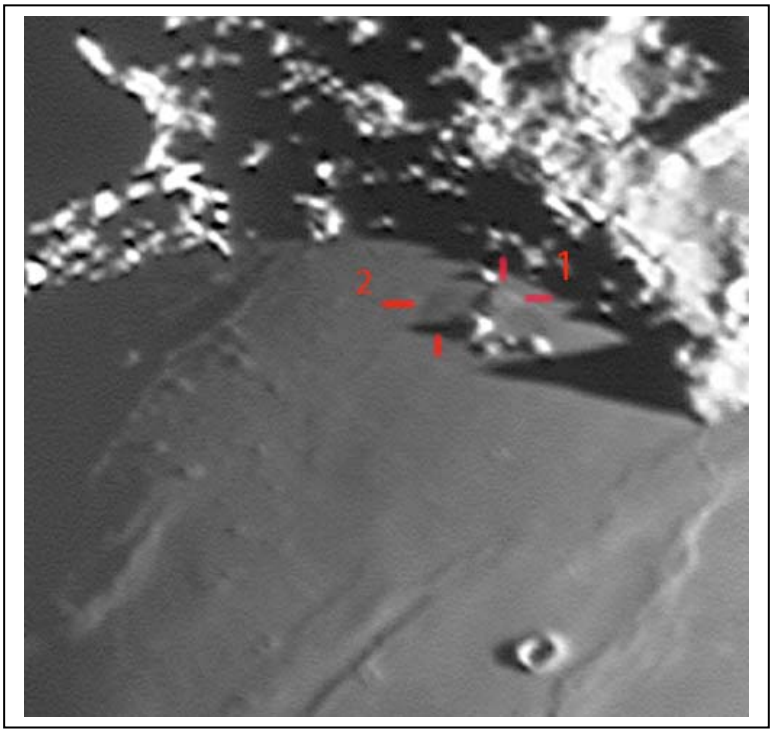

Fig.1: K.C.Pau on July 16, 2005,at 13:27 UT (H = 2.70°,C=30,98°)

eastern edge. No lunar domes are reported near Promontorium Laplace in the ALPO catalogue and the revised list of lunar domes (Kapral and Garfinkle, 2005). USGS lunar geologic map I-602 (Schaber, 1969) reports a dome as an Id unit at 27.83° W and 40.66° N, nearly 200 km to the south.

In this study we report measurements and include CCD images of two previously unlisted lunar domes, named Laplace 5 and Laplace 6, which will be included into the lunar dome catalogue by Kapral and Garfinkle (2005). The first is located at 28.66° W and 47.17° N (Xi −0.326, Eta +0.733) and the second is a shallow dome located to the west at 29.16° W and 47.08° N (Xi = −0.332, Eta = +0.732). Table 1 lists the seven observers and their instruments. For each of the observations in Table 1, the local lunar altitude H of the Sun and the selenographic colongitude C were calculated using the Lunar Observer's Toolkit by H. D. Jamieson. All images are oriented approximately with north at the top and west (IAU) to the left.

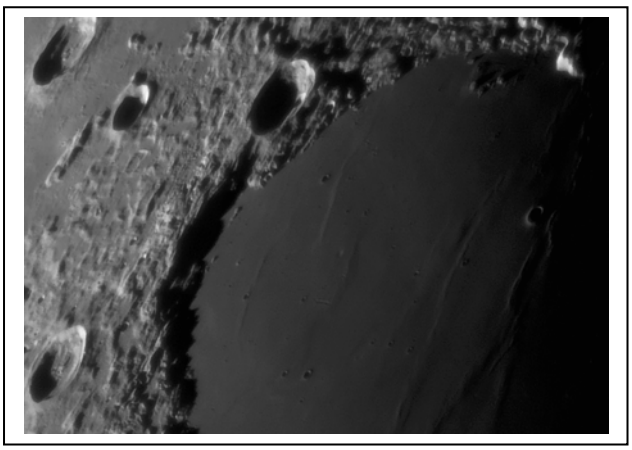

Fig.2: Paolo Lazzarotti on October 27, 2005, at UT (H = 3.11°, C = 203.45°).

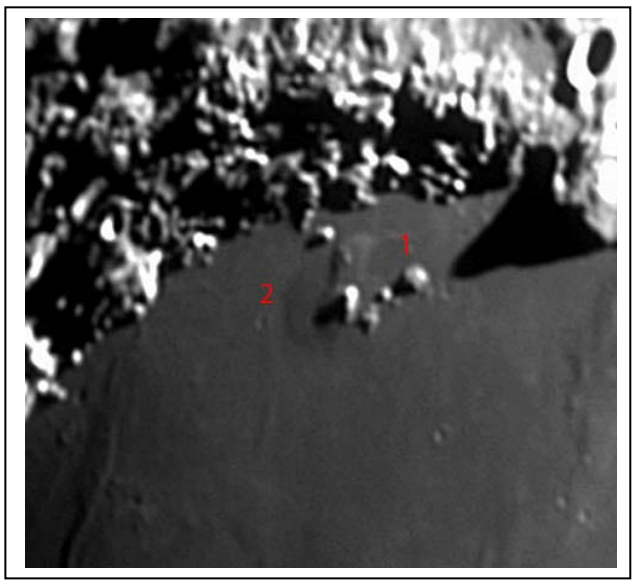

Fig.3: Jim Phillips on November 12, 2005, at 04:58 00:40 UT (H = 4.51°, C = 36.32°).

2. Observations

Using our available images (Table 1), the diameter of dome 1, corrected for foreshortening, is 9.0 ± 0.5 km. This structure, located at 28.66° W and 47.17° N, requires a specific solar altitude to be observed clearly, "disappearing" under higher illumination angles.

Figure 1 displays the dome Laplace 5 under a low solar altitude (2.70°). Figure 2 was taken at a slightly higher sun angle (3.11°) and the eastern flank of the dome does not show a black shadow in the raw image, but a dark grey shading. Figure 3 was taken under a solar angle of 4.51°. Another image (Figure 4) was taken at a lower sun angle of 2.80° and reveals a shallow, possibly intrusive structure to the west of Laplace 5, to which we assigned the name Laplace 6. Figure 5 displays the dome Laplace 5 under a low solar altitude of 2.99° while Figure 6 was taken under a solar altitude of 5.04°.

Table 1: Observations of the two domes located at (28.66° W, 47.17° N) and (29.16° W, 47.08° N).

Observer	Telescope	Camera	UT date and time	Solar altitude H	Height (m)	Slope (°)	Figure
Baldoni P. & Cellini C.	Newtonian 260 mm f/5	Philips ToUCam	September 25, 2005 (04:52)	23.35°			
Lazzarotti P.	Dall-Kirkham 315 mm f/25	CCD Lumenera Infinity	October 27, 2005 (04:58)	3.11°	125 ± 15	1.6 ± 0.2	2
Lena R.	Refractor APO 130 mm f/6	Visual and Philips ToUCam	November 11, 2005 (19:45)	2.84°			
Pau K. C.	Newtonian 250 mm f/6	Philips ToUcam	July 16, 2005 (13:27) October 13, 2005 (12:39)	2.70° 5.56°	130 ± 20	1.65 ± 0.25	1
Phillips J.	Refractor APO 200 mm f/9	CCD Atik	November 12, 2005 (00:40) January 10, 2006 (02:24)	4.51° 2.99°	140± 20	1.8 ± 0.2	3 5
Sbarufatti G.	Schmidt-Cassegrain 200 mm f/10	Philips Vesta Pro	September 8, 2004 (00:39) July 30, 2005 (02:27)	9.60° 9.50°			
Wöhler A. & C.	Newtonian 200 mm f/6	Philips ToUCam	October 23, 2004 (19:37) December 11, 2005 (17:35)	2.80° 5.04°	120± 20	1.5 ± 0.3	4 6

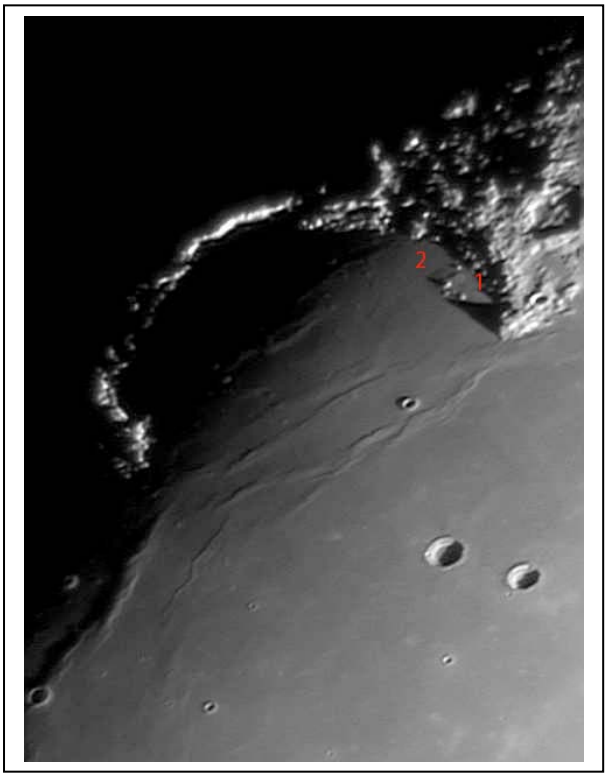

Fig.4: Alexander and Christian Wöhler on October 23, 2004, at 19:37 UT.

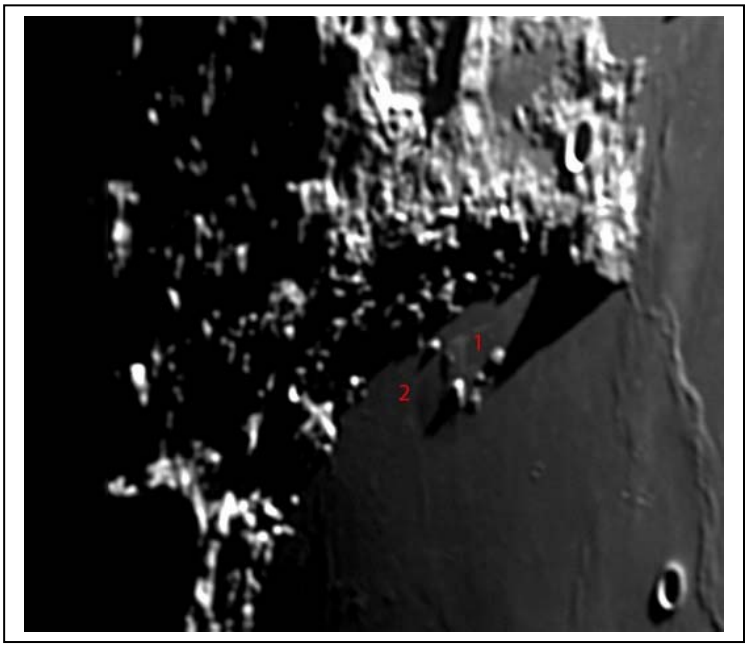

Fig.5: Jim Phillips on January 10, 2006, at 02:24 UT (H = 2.99°, C = 35.47°).

3. Morphologic, morphometric, and spectral properties

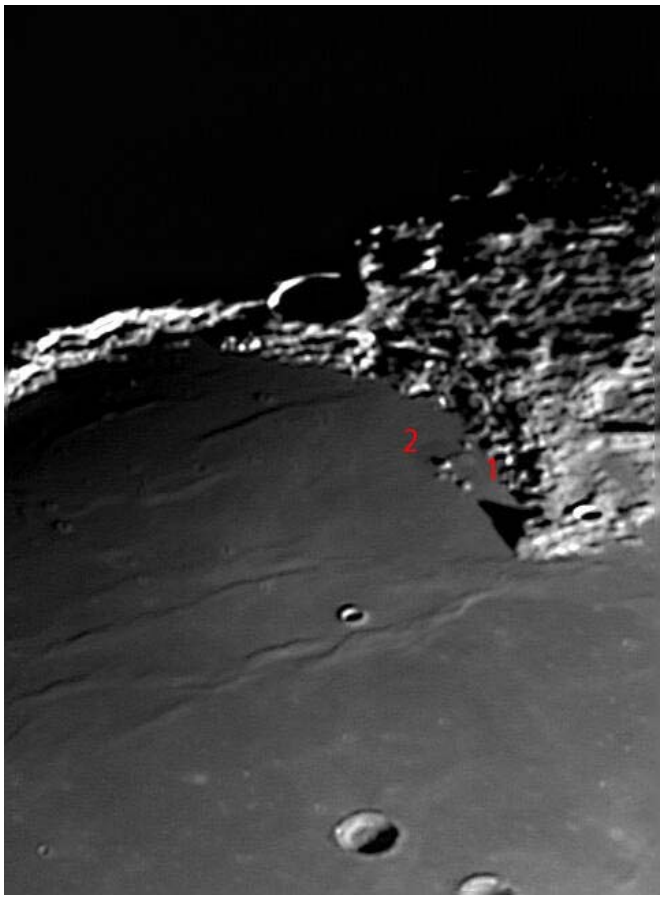

Fig.6: Christian Wöhler on December 11, 2005, at 17:35 UT (H = 5.04°, C = 37.67°).

The height values for dome Laplace 5 (Table 1) were derived by a combined photoclinometry and shape from shading analysis (Horn, 1989; Wöhler et al, 2006; Lena et al., 2006, and references therein) and shadow length measurements performed based on Figure 5. The 3D reconstruction of dome Laplace 5, obtained based on Figure 2, is shown in Figure 7. The height values reported in Table 1 for Laplace 5 were obtained by determining elevation differences between the summit of the dome and its surrounding on the corresponding 3D profiles derived by photoclinometry and shape from shading analysis. The dome height on the images shown in Figures 1 and 2 was measured as 130 ± 20 m and 125±15 m, respectively. These height values are consistent with the measurements carried out on the image shown in Figure 4, yielding 120 ± 20 m, and Figure 5, resulting in 140±20 m. From Table 1 it follows that the average slope angle of the dome is smaller than 2°, corresponding to a dome having a gentle slope. The height of the dome, located at 28.66° W and 47.17° N, was also computed from Figure 5 using the shadow length method according to the relation:

$h = l \tan H$, where l is the shadow length, corrected for foreshortening and measured in km, and $\tan H$ the tangent of the solar altitude. A height of 115 ± 15 m was obtained, resulting in an average slope of 1.5° ± 0.10°. This value is slightly lower than the height values obtained with the photoclinometry and shape from shading method since the shadow only partially covers the western flank of the dome and therefore does not account for the full dome height.

The dome edifice volume was determined according to the relation $V = (\pi/2)\,[h\,(D/2)^2]$, assuming a parabolic shape (Wilson and Head, 2003). We thus obtain an edifice volume of 4.1 km³.

The Clementine UVVIS spectral data reveal for the dome Laplace 5 a rather high 750 nm reflectance of R_{750} = 0.1205, an extraordinarily low value for the UV/VIS colour ratio of R_{415}/R_{750}=0.5553, indicating a low TiO_2 content, and a weak mafic absorption with R_{950}/R_{750}=1.029 suggesting a high soil maturity.

Laplace 6 is a shallow, possibly intrusive structure situated just to the west of Laplace 5 at 29.16° W and 47.08° N.

From Figures 4 and 5 the dome radius (summit to bottom at its western edge) of the shallow structure is 7.7±0.6 km. The height was determined to 110 ± 20 m in Figure 4 and to 80 ± 15 m in Figure 5, corresponding to a flank slope of 0.8°±0.15° and 0.6°±0.1°, respectively.

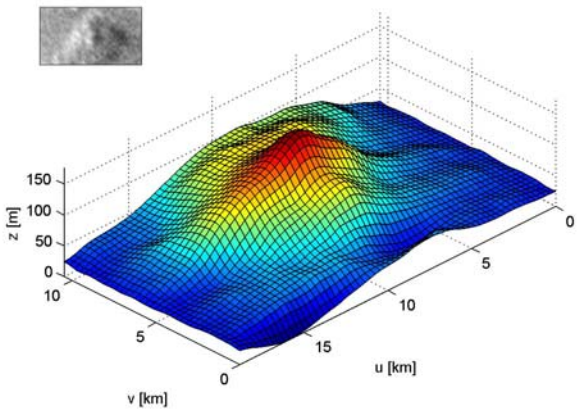

Fig.7: The 3D reconstruction of dome 1, obtained based on Figure 2.

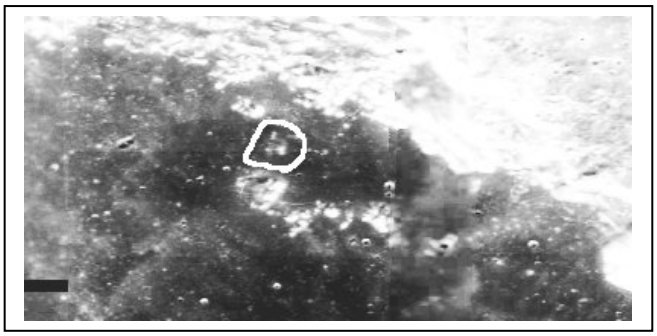

Fig.8: Clementine 750 nm image.

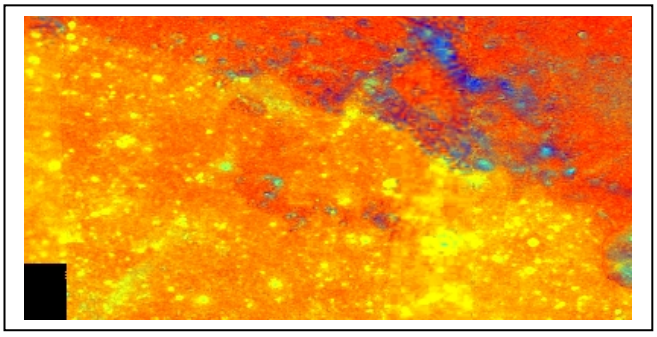

Fig.9: Clementine UVVIS imagery, colour ratio.

4. Rheologic modelling

We assume that the dome Laplace 5 was formed by extrusion of magma onto a flat plane spreading in all directions from the vent, in contrast to lava flows resulting from lava extrusion onto an inclined surface. Wilson and Head (2003) provide a quantitative treatment of such dome-forming eruptions. This model estimates the yield strength τ, i. e. the pressure or stress that must be exceeded for the lava to flow, the plastic viscosity η,yielding a measure for the fluidity of the erupted lava, the effusion rate E, i. e. the lava volume erupted per second, and the duration:

T = V/E of the effusion process. This model is applied to a large set of representative lunar mare domes by Wöhler et al. (2006). It relies on the morphometric dome properties (diameter, height, volume) and several physical constants such as the lava density, the acceleration due to gravity, and the thermal diffusivity of the lava. The computed values for τ, η, E, and T obtained with the model by Wilson and Head (2003) are valid for domes that formed from a single flow unit (monogenetic volcanoes). Otherwise, the computed rheologic values are upper limits to the respective true values.

The low slope and large diameter of the dome regarded in this study suggest a high effusion rate, a low lava viscosity, and a short duration of the effusion process.

The rheologic model by Wilson and Head (2003) yields an effusion rate of 111 m^3/s. It formed out of lava with a moderate viscosity of 2.4 x 10^5 Pa s over a period of time of 1.2 years. The model was not applied to the shallow dome Laplace 6 because it is probably an intrusive structure.

5. Results and discussion

The dome Laplace 5 is an effusive dome, and a crater pit may be present on its summit. Several small prominences (see Figures 1-6) represent hummocky material units likely embayed by the dome. In the Clementine 750 nm image (Figure 8) these features appear as three bright spots located near the centre of the dome, but most of the dome surface is as dark as the surrounding surface, mapped as an Im2 unit in the USGS map I-602 and assigned as Imbrian in age. Using the rheologic model described by Wilson and Head (2003), we obtain an effusion rate of 111 m^3/s. Laplace 5 formed out of lava with a moderate viscosity of 2.4 x 10^5 Pa s over a period of time of 1.2 years, yielding a low edifice volume of 4.1 km^3.

Laplace 6 is a shallow structure, and possibly it may represent a lava bulge or also a low domical structure of intrusive nature, e. g. a subsurface intrusion similar to a terrestrial laccolith, where magma has flowed under a surface of solidified lava and lifted it up (Head and Gifford, 1980).

Clementine UVVIS imagery reveals that the two domes, like the surrounding mare, spectrally appear extremely red and have thus formed in basalts of low TiO_2 content (Figure 9).

According to the novel GLR classification scheme for effusive domes (Table 2) developed by Wöhler et al. (2006) based on the spectral properties and 3D shapes of a set of 38 effusive lunar mare domes, Laplace 5 is a B_2 dome due to its moderate lava viscosity, its spectrally red appearance suggesting a low TiO_2 content, and the high lava effusion rate.

Table 2: Approximate spectral and morphometric properties characterising the dome classes A-D described by Wöhler et al (2006) and an additional class G for lunar highland domes.

Class	TiO_2 content	R_{415}/R_{750}	Slope [°]	D [km]	V [km^3]
A	high	> 0.64	0.3-1.0	5-13	< 3
B_1	largely moderate	0.55-0.64	2.0-5.4	6-15	5-32
B_2	largely moderate	0.55-0.64	1.3-1.9	8-15	2-21
C_1	low to moderate	0.55-0.60	0.6-1.8	13-20	7-33
C_2	moderate to high	0.60-0.64	1.0-2.5	8-17	4-17
D	high	> 0.64	1.3-2.5	≈ 25	40-67
G	low to moderate	0.55-0.60	> 6.0	7-30	20-390

References

[1] Head, J. W., Gifford, A., Lunar Domes: Classification and Modes of Origin, Moon and Planets, vol. 22, pp. 235-258, 1980.

[2] Horn, B. K. P., Height and Gradient from Shading, MIT technical report, AI memo no. 1105A, 1989. http://people.csail.mit.edu/people/bkph/AIM/AIM-1105A-TEX.pdf

[3] Jamieson H. D., Toolkit. http://home.bresnan.net/~h.jamieson/

[4] Kapral, C., Garfinkle, R., 2005. GLR Lunar Dome Catalog.
http://www.glrgroup.org/domes/kapralcatalog.htm

[5] Lena, R., Wöhler, C., Bregante, M.T., Fattinnanzi, C., A combined morphometric and spectrophotometric study of the complex lunar volcanic region in the south of Petavius, JRASC 100(1), 14-25, 2006.

[6] Schaber, G. G., Geologic Map of the Sinus Iridum Quadrangle of the Moon, USGS, Lunar geologic map I-602, 1969.

[7] Wilson, L., Head, J. W., Lunar Gruithuisen and Mairan domes: Rheology and mode of emplacement, J. Geophys. Res. 108(E2), 5012-5018, 2003.

[8] Wöhler C., Lena R., Lazzarotti P., Phillips J., Wirths M., Pujic Z., A combined spectrophotometric and morphometric study of the lunar mare dome fields near Cauchy, Arago, Hortensius, and Milichius, Icarus, in press, 2006.

NEW SPECTROPHOTOMETRIC AND MORPHOMETRIC LUNAR DOME CLASSIFICATION – SUMMARY –

by Jim Phillips and Raffaello Lena - Geological Lunar Research GLR (group)

In an article currently in press in the journal "Icarus", titled *A Combined Spectrophotometric and Morphometric Study of the Lunar Mare Dome Fields near Cauchy, Arago, Hortensius, and Milichius*, Wöhler et al. (2006) have described a new classification scheme for effusive lunar mare domes complementary to the previous scheme by Head and Gifford (1980). These data are based upon analysis of dome fields near Cauchy, Arago, Hortensius, and Milichius. Clementine UVVIS multispectral data obtained at five wavelengths (415, 750, 900, 950 and 1000 nm) for soil composition analysis, in particular TiO_2 content, high resolution CCD earth based imaging, 3D image reconstruction based upon shadow analysis and photometric evaluation of calibrated image pixel intensities, form the basis for this new classification scheme. Approximation of high, moderate and low TiO_2 content is based on the

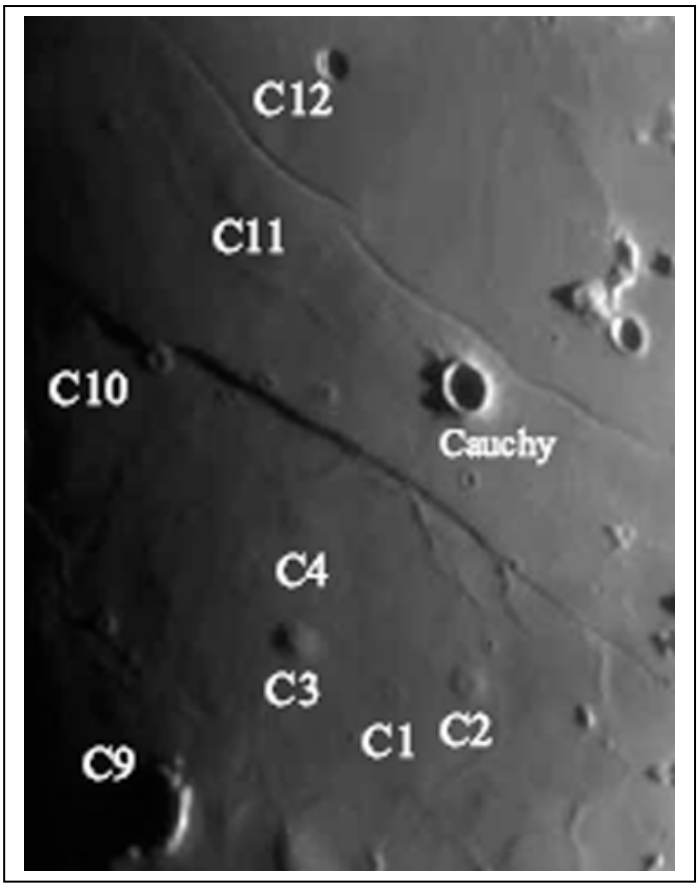

Fig.1: Cauchy (C) dome field, with domes C1–C4 and C9–C12.

ratio of the reflectances R_{415} at 415 nm and R_{750} at 750 nm as follows:

Low TiO_2 content: $R_{415}/R_{750} < 0.60$

Moderate TiO_2 content: $0.60 < R_{415}/R_{750} < 0.64$

High TiO_2 content: $R_{415}/R_{750} > 0.64$

The new classification is broken down into 4 mare dome categories with 2 categories further subdivided as follows:

Class	TiO_2 content	R_{415}/R_{750}	Slope [°]	D [km]	V [km^3]
A	high	> 0.64	0.3-1.0	5-13	< 3
B_1	largely moderate	0.55-0.64	2.0-5.4	6-15	5-32
B_2	largely moderate	0.55-0.64	1.3-1.9	8-15	2-21
C_1	low to moderate	0.55-0.60	0.6-1.8	13-20	7-33
C_2	moderate to high	0.60-0.64	1.0-2.5	8-17	4-17
D	high	> 0.64	1.3-2.5	≈ 25	40-67
G	low to moderate	0.55-0.60	> 6.0	7-30	20-390

Class A: domes are shallow, small domes formed by low viscosity lavas of high TiO_2 content erupting at high effusion rates over very short periods of time.

Class B_1: domes have steep flank slopes and formed from lavas of moderate TiO_2 content erupting at low to intermediate effusion rates over a long period of time.

Class B_2: domes formed during shorter periods of time than those of class B_1 resulting in shallow flanks with lower volumes.

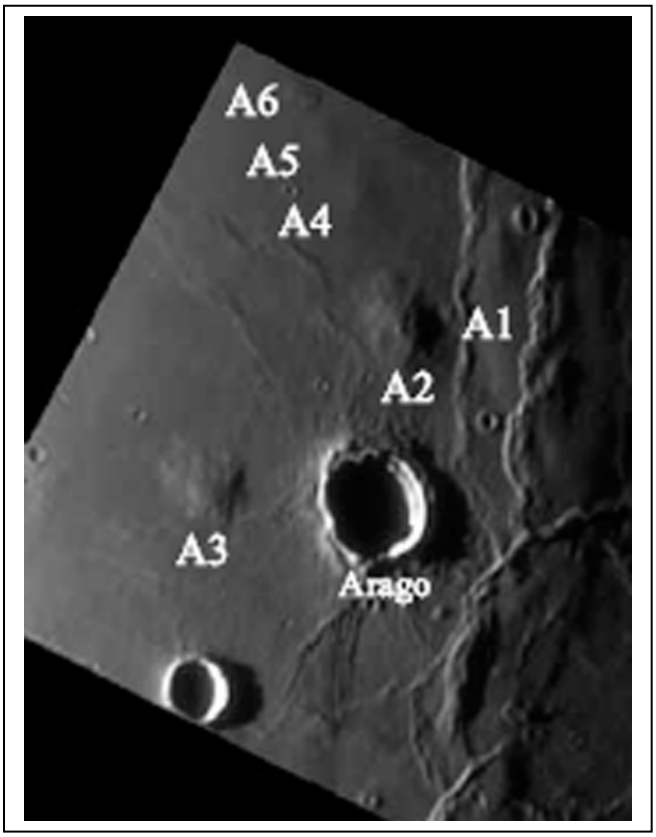

Fig.2: Arago (A) dome field, with domes A1 – A6.

Class C_1: domes have a low TiO_2 content and were formed by low viscosity lavas at high effusion rates resulting in large diameters and shallow flanks (pancake shapes).

Class C_2 : domes are similar to C_1 but with high TiO_2 contents.

Class D: domes are very complex, large, shallow, voluminous domes such as Arago Alpha and Beta as well as several domes in the Marius Hills region, which likely formed during several stages of effusion.

Class G: is an additional class, not explicitly mentioned by Wöhler et al. (2006), representing large, steep and voluminous highland domes such as the Gruithuisen and Mairan domes.

Future studies on additional dome fields containing both effusive and intrusive domes and more complex structures like those in the Marius Hills region will be forthcoming.

Examples are as follows:

Class A: Arago 1, 4 and 5. Cauchy 1, 4. See Figure 2

Class B_1: Hortensius 2, 3, 4, 5, 6 and Milichius 11 and 12. See Figures 3 and 4

Class B_2: Hortensius 1, 7. See Figure 3

Class C_1: Milichius 1, 2, 3, 5, 6 and 10. See Figure 4

Class C_2: Cauchy 2, 3. See Figure 1

Class D: Arago 2 and 3 (Alpha and Beta). See Figure 2

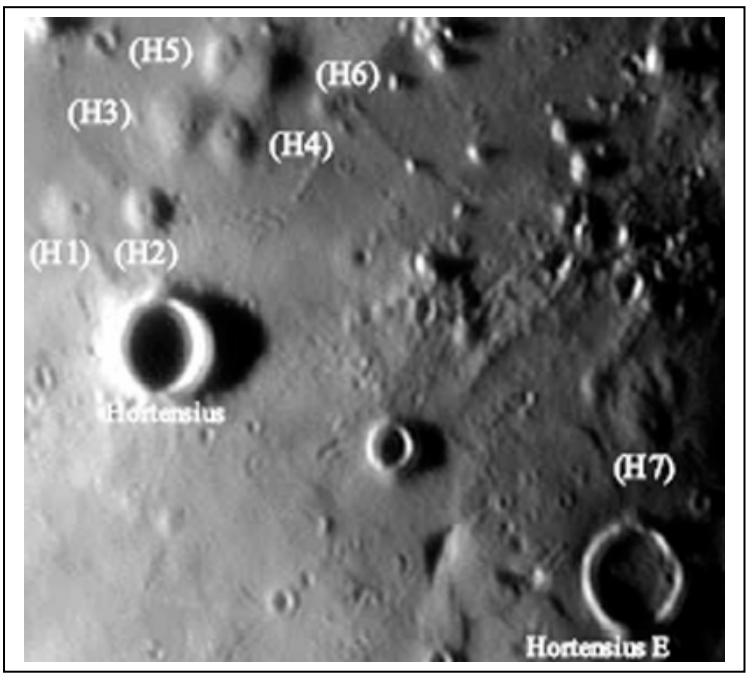

Fig.3: Hortensius (H) dome field, with domes H1- H7.

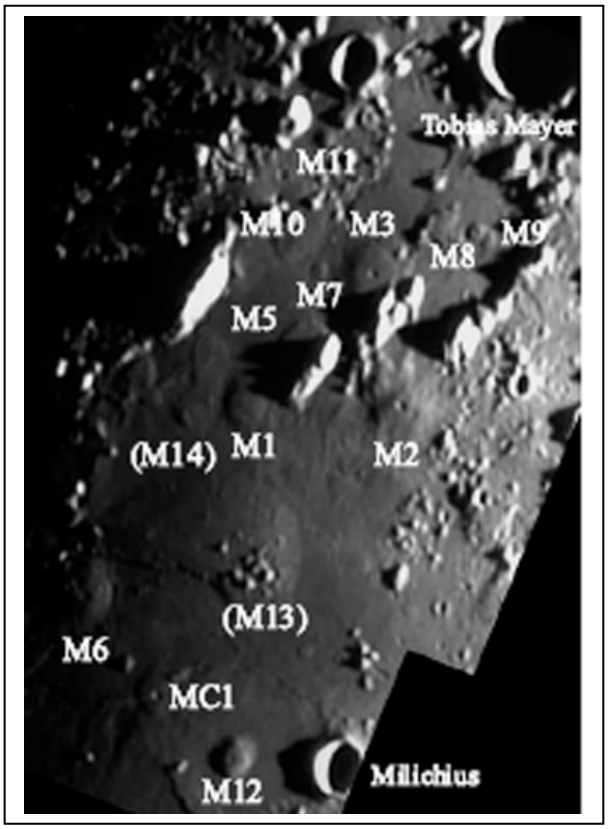

Fig.4: Milichius (M) dome field, with dome:M1-M3 and M5-M14With MC1 are indicated two cones near Milichius.

References

[1] Head, J. W., Gifford, A., Lunar Domes: Classification and Modes of Origin, Moon and Planets, vol. 22, pp. 235-258, 1980.

[2] Wöhler, C., Lena, R., Lazzarotti, P., Phillips, J., Wirths, M. and Pujic, Z., A Combined Spectrometric and Morphometric study of the Lunar Mare Dome Fields near Cauchy, Arago, Hortensius, and Milichius, Icarus, in press, 2006.

THE MOON ON A SPREADSHEET: PHOTOCLINOMETRY USING EXCEL

by Richard Evans - Geological Lunar Research GLR (group)

Abstract

Photoclinometry, the measurement of the height of lunar features using shading, is a complex field and many different algorithms and reflectance functions have been used by professionals to estimate the height of lunar features. The simplest methods assume Lambertian reflectance but the Moon is not a pure Lambertian reflector. If it were, the limb of the full Moon would be dark, not the bright limb that we see. The most accurate photoclinometric methods involve algorithms that invoke many parameters to account for the Moon's peculiar reflectance properties and these are generally called Lunar Lambertian reflectance methods. ISIS, a Linux based program used by many astronomers to process photoclinometric data from satellites and probes is such a program and is in the public domain. However, at present ISIS requires that many parameters be encoded within the image itself and it is not well suited to the needs of the amateur. The GLR group has been able to make very accurate photoclinometric measurements of lunar features using a complex Lunar Lambertian algorithm (Wöhler et al., 2006). However, software is not available to make this method generally accessible and some parameters (Hapke parameters) must be determined manually by reference to graphs. This paper describes the manual application of a simple shape from shading algorithm to eleven lunar domes using Microsoft's ubiquitous spreadsheet program EXCEL. This program is used in conjunction with two freeware programs: ImageMagick-6.2.5 and ImageJ. The purpose of this paper is two-fold: to perform photoclinometric measurements of lunar domes using EXCEL and to compare approximations obtained with a simple Lambertian algorithm to published results obtained using a more definitive Lunar Lambertian model (Wöhler et al., 2006).

1. Introduction

The first step in the process is the conversion of the image file into a txt document which is then imported into EXCEL. A shape from shading transform is then applied to the data using a series of Macro functions within EXCEL. This process results in the generation of a Lambertian transform data map whose data points yield the height of surface pixels when multiplied by the resolution of the original image in meters/pixel. A greyscale data map is also produced and upon conversion into an image, this map yields a digital elevation map of the lunar feature.

This method has many advantages. First, the specific shape from shading algorithm used is a known factor.

This is not always the case with commercial shape from shading filters. Second, the user has the ability to substitute shape from shading transforms at will. Third, the transformation process preserves the row/column data presentation of the original image. This allows rapid plotting of feature heights along any desired row in the original image. Finally, the production of a digital elevation map (DEM) from the original image allows rapid visual assessment and feature height from pixel value determinations. Furthermore, the DEM can be imported into a computer aided design program or similar software to allow three dimensional visualization of a topographic map generated from the DEM data.

2. Selection of a Photoclinometric Algorithm

Many algorithms exist for determination of feature height from the pattern of shading that results from oblique illumination. These algorithms are based on the type of reflectance exhibited by the feature under consideration. Surfaces with perfectly matte properties typically reflect incident light according to Lambert's cosine law which states that the intensity of reflected or transmitted light on such a surface will vary as the cosine of the angle between the direction of illumination and the vector normal to (i.e. perpendicular to) the surface. For the Moon, therefore, intensity varies with the cosine of the zenith angle of the sun, which is given by subtracting the local solar elevation from 90 degrees. For a surface with Lambertian reflectance, luminance is the same at any viewing angle. However, the Moon is not a pure Lambertian reflector. Even so, under certain conditions, lunar reflectance can be closely approximated by Lambert's law. Summarizing these conditions:

1) the lunar surface under study must be within the area bounded approximately by the 30 degree longitude and latitude lines (not too close to the lunar limb)

2) solar lighting of the lunar surface must be oblique (solar elevation should not exceed 20–30 degrees)

3) the surface should not vary excessively in albedo (reflectance properties should be uniform across the surface)

3. The Carlotto Algorithm

For the present study, I chose an algorithm described by Carlotto (1996). This algorithm greatly simplifies the complex calculations required for height determination. The algorithm can only provide an approximation to the more definitive Lunar Lambertian reflectance function and it will tend to slighly underestimate the height of lunar features. Remember that the Moon is not a pure Lambertian reflector (again, if it were then the full Moon would have a dark limb). The principles underlying the algorithm are explained by Horn (1977), Horn (1979), Horn (1990), and Carlotto (1996). The lunar feature under study must conform to the conditions described above which favor Lambertian type reflectance. The algorithm is based on Carlotto's observation that:

Eq. 1 $i(x,y) \sim a [\sin(s)\, p(x,y) + \cos(s)]$

where i(x,y) is the pixel intensity, s is the zenith angle of the sun, p(x,y) is the horizontal surface slope, and a is a constant scale factor dependent on albedo. However, when illumination is directly down rows in the image then the average gradient in the x direction is zero by definition and:

Eq. 2 $E[i] \sim a \cos(s)$.

Where E(i) is the average pixel value. It is then possible to approximate the scale constant a:

Eq. 3 $a = E[i] / \cos(s)$

Therefore, there is a requirement that all illumination of the surface under study be from the left (i.e. 270 degrees) so that light shines directly down pixel rows in the image. This requirement can also be fulfilled by rotation of the image to achieve the same effect.

Carlotto then determines the elevation map z(x,y) iteratively by a rolling summation:

Eq.4 $z(x,y) = z(x-1,y) + [i(x,y) - a\cos(s)]/[\sin(s)]$

This implies that

Eq. 5 $Eg = (Pv - AvgPv)/(AvgPv * \tan(s))$

Where Eg is the elevation gradient at a pixel whose pixel greyscale value is Pv and whose average row pixel value is AvgPv. The elevation z(x,y) of the pixel is given by the summation of the individual Eg values of all preceeding pixels in the same row.

4. Photoclinometric Analysis Using EXCEL

Step 1: Imaging

The image of the lunar feature should be greyscale and in either jpg or bmp format. The intensity of incident light in the image is expected to be proportional to the greyscale value of the pixel, but CCD cameras usually allow manual adjustment of gamma values. The greyscale value of a pixel is actually proportional to the light intensity raised to the power of the gamma value. If desired, the accuracy of the camera gamma scale can be ascertained by performing a calibration using flatfield images taken under different light intensities and different neutral density filters. Lena et al. (2005) determined that gamma scale error was about +/- 0.1 for the Philips ToUCam.

The date and time the image was taken and the longitude/latitude of the feature imaged are used to determine the local lunar solar elevation, azimuth, and zenith angle. These values may be obtained using H. D. Jamieson's Lunar Observer's Toolkit (ALPO) or an analogous program. The zenith angle is obtained by subtracting the local solar elevation from 90 degrees. The resolution of the image in meters per pixel is determined by referencing a feature of known size within the image.

The image must be rotated until the direction of incident light is directly from the left (i.e. 270 degrees). After the rotation, the image should be cropped to a rectangular shape.

Step 2: Converting the image into a txt data file and importing it into EXCEL

Conversion of the image file into a txt data file can be accomplished with the public domain program ImageMagick-6.2.5 which runs from the command prompt. With the image file image.jpg in the ImageMagick directory, the command takes the form: convert image.jpg TEXT:image.txt

The txt data file is then imported into an EXCEL workbook as a worksheet named TxtData. This worksheet should contain three data columns which record the x value, y value, and greyscale value for each pixel.

Step 3: Defining Keyboard Macro Subroutines in EXCEL

This step requires the creation of several short uncomplicated Macro subroutines in Excel. These subroutines will calculate the average pixel greyscale value for each row, apply the Lambertian transform, perform a rolling (i.e. iterative) summation of the transform gradients along each row, and calculate greyscale values for a digital elevation map for each row.

Macros are executed by holding down the Control Key while pressing a keyboard letter that engages the desired macro subroutine. The Visual Basic Script for each keyboard Macro used in the sample calculation for the Cauchy Omega dome is listed in Appendix 1. Adapting these Macros for use on other images will require minor adjustments to the Range values since these depend on the number of pixels in a row. For individuals not very familiar with EXCEL and keyboard Macros, a more detailed procedural description has been provided in Appendix 2.

Step 4: Generating Transform Summation and DEM Greyscale Data Maps

Running the Macros described above sequentially yields Transform Summation and DEM Greyscale Data Maps for each row. These rows are copied and manually pasted to separate spreadsheets named TransSum and DEM using the Special Paste command (a short Macro can be written to perform the Special Paste function more rapidly). Row after row, the Transform Summation and DEM Greyscale Data Maps are generated in this way. The graphing function in EXCEL can be rapidly used to generate x,z plots along any desired y row. The feature height is given by the feature height in pixels on the plot multiplied by the image resolution in meters/pixel.

Step 5: Generating a DEM Image from the DEM Greyscale Data Map:

The Transform Summation map is used to generate the DEM Greyscale Data Map by adding an arbitrary constant and multiplying the result by a second arbitrary constant. The constants are chosen to make maximum use of the 0 to 255 limits of the greyscale (i.e. to obtain the best distribution within the 0 to 255 limits possible). The resulting Greyscale data map is exported from EXCEL as a tab delimited txt file. This file is then imported into a program such as ImageJ as a txt image file. It may then be saved in jpg, bmp, tiff or other desired format. The image file represents a digital elevation map of the feature. The image is converted to color mode (the red, blue and green values will all be the same) and pixel values at any point will yield the feature elevation if adjusted for the scale amplification introduced by the two constants described above.

The DEM image can be imported into a computer assisted design program such as Rhino 3.0 (a NURBS modeling program) as a heightfield map and utilized to generate a three dimensional topographic map of the lunar feature. Many other software products perform similar 3D topographic visualization functions as well.

Step 6: Correcting Feature Height for Image Distortion

If the image is not in cylindrical projection then the pixel scale has to be adjusted by $1/\cos L_0$ in the east-west direction and by $1/\cos B_0$ in the north-south direction where B_0 is the effective selenographic latitude of the feature with respect to the sub-earth point and L_0 is the effective selenographic longitude of the feature with respect to the sub-earth point.

As an alternative, the image can be put into cylindrical projection using the free program IRIS by applying the MAP command.

Step 7: Find Contribution to Dome Height made by Curvature of the Lunar Surface

Refer to the diagram below. The diameter of a lunar dome represents an arc ab across the lunar surface.

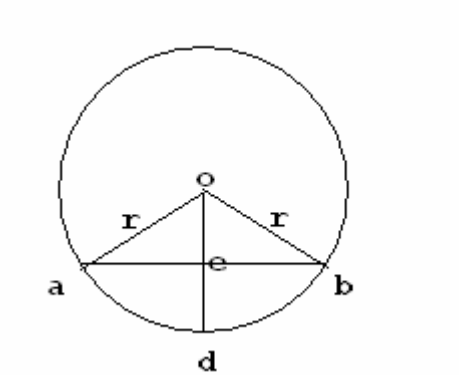

1. The central angle subtending that arc (i.e. aob) is given by:

dome diameter: * 180/(π * r) where r is the mean lunar radius

2. The angle oae is given by 180 – 90 – (aob/2)

sine (oae) = oe/r

r – oe = ed where ed is the contribution to dome height made by lunar curvature alone

The calculations above should be done to 7 significant figures

5. Sample Calculation:

Cauchy Omega Dome (Image by Paolo Lazzarotti, GLR Group)

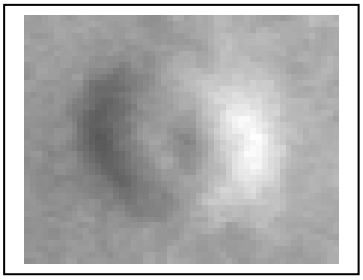

Fig.1: Cauchy Omega dome.

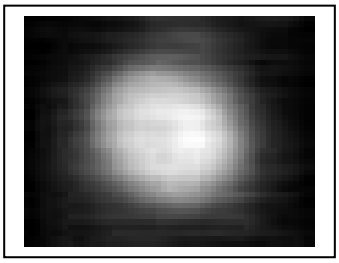

Fig.2:Cauchy Omega dome, digital elevation map.

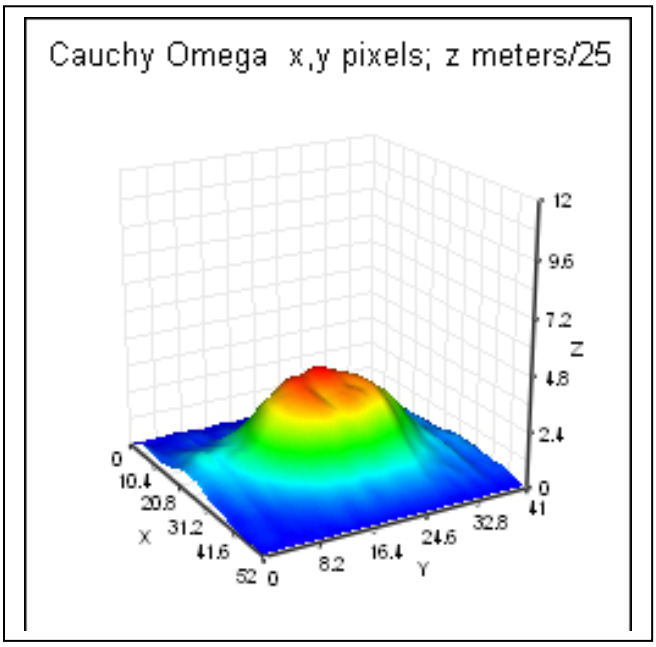

Fig.3: Cauchy Omega dome, 3D plot.

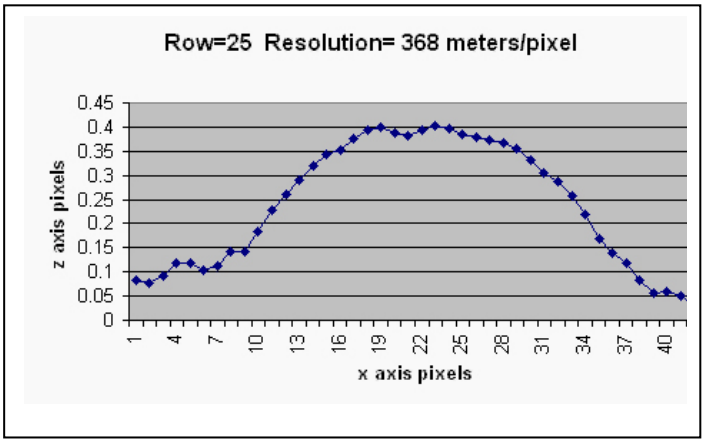

Fig.4: Cauchy Omega dome, Excel plot.

Figs.1.3: 38.32 East Longitude 7.23 North Latitude; Elevation 4.19 degrees; Azimuth 270 degrees; Zenith Angle 85.81 degrees; Gamma 1.0; Resolution 368 meters/pixel

Fig.4: Height is 95.3 meters. Error bars of 10% can be applied due to anticipated errors in camera calibration. The contribution to dome height caused purely by lunar curvature is 15.6 meters.

Results for ten additional lunar domes have been placed in Appendix 1.

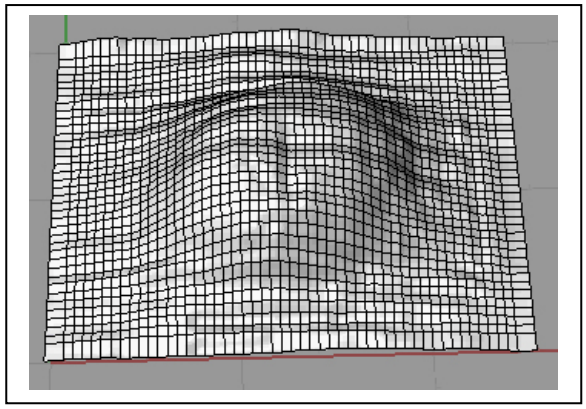

Fig.5:Cauchy Omega dome, topographic plot of digital elevation map in Rhino 3.0 with height scale 3.0x.

6. Comparison of Data with Dome Heights Cited by Wöhler et al. (2006):

Table 1 Excel plot of dome height data for present study as compared with data for identical domes given by Wöhler et al. (2006).

	Longitude	Latitude	Height meters [a1]	Height meters [a2]	Height meters [b]	Diameter (km) [a]	Diameter (km) [b]
Cauchy Omega	38.32	7.23	95.3 ± 9.5	110.9 ± 11	125 ± 15	12.1 ± 1.2	12.2
H01 near Hortensius	-28.41	7.18	117.8 ± 12	123± 12	140 ± 14	8.7 ± 0.87	-----
H07 near Hortensius	-25.17	6.07	89.37 ± 8.9	96± 9.6	100 ± 10	9.8 ± 0.98	-----
Arago Alpha	21.7	7.56	282 ± 28	328.4 ± 32.8	330 ± 30	25.3± 2.5	25.4
Cauchy Tau	36.73	7.58	174.1± 17	190.28 ± 19	190 ± 19	15.0 ± 1.5	-----
Milichius Pi	-31.2	10.08	214.5± 21	224.5 ± 22	230 ± 23	11.85 ± 1.2	-----
Arago Beta	20.07	6.24	264.1± 26	282.5 ± 28	270 ± 27	16 ± 1.6	-----
H02 near Hortensius	-28.01	7.12	201.1 ± 20	204.87 ± 21	230 ± 23	7.2 ± 0.72	-----
M03 near Milichius	-30.43	13.78	189.52 ± 19	192.99 ± 19	190 ± 10	12.43 ±1.2	-----
Y01 near Yerkes	49.96	14.82	101.29 ± 10	112.7 ± 11	110 ± 10	12.6 ± 1.3	-----
A01 near Arago	21.96	7.66	35.78 ± 3.6	37.92 ± 3.8	40 ± 4	5.46 ± 0.55	-----

[a1]= present study, **includes subtraction of contribution to lunar height due to lunar curvature**
[a2]= present study, does not include subtraction of contribution to lunar height due to lunar curvature

[b]= data from previous GLR studies summarized in Wöhler et al. (2006) using a Lunar Lambertian algorithm (includes subtraction of contribution to lunar height due to lunar curvature)

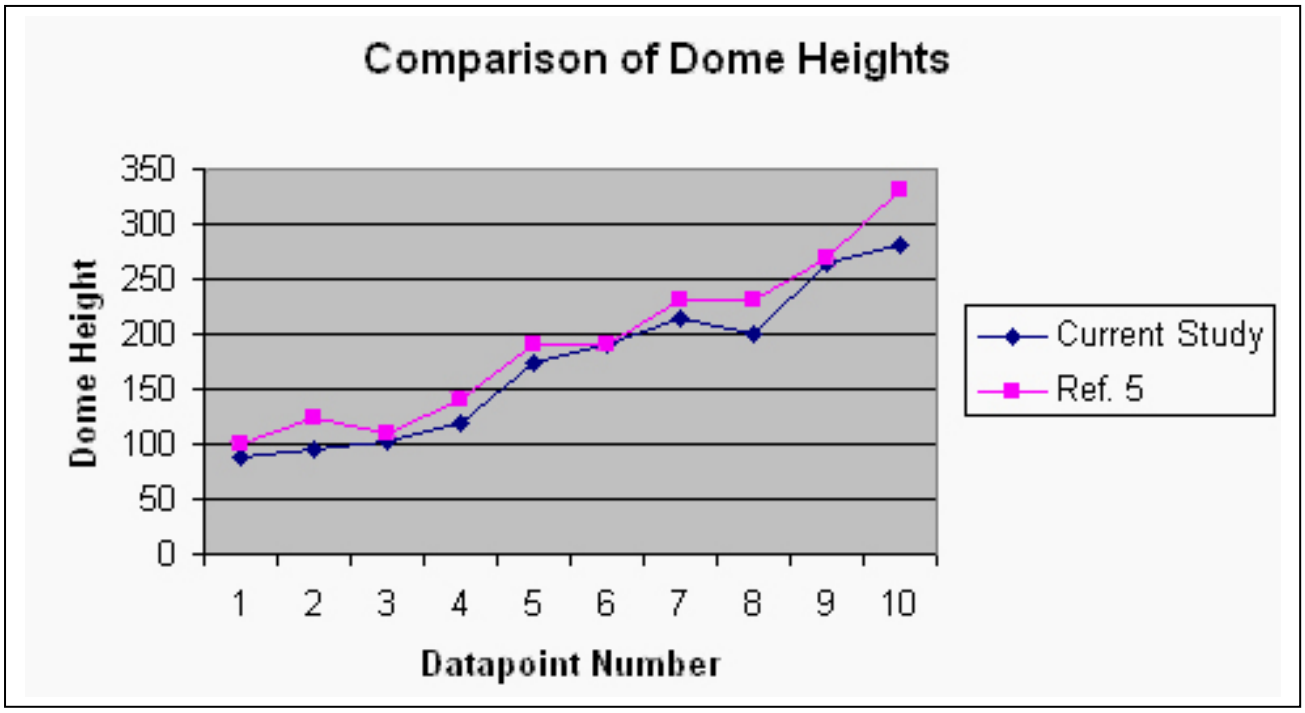

Fig.6: Comparison of Dome Heights, Excel Plot of current data against dome data given by Wöhler et al. (2006).

Where 1=A01; 2= H07; 3=Cauchy Omega; 4=Y01; 5=Dome H01; 6=Cauchy Tau; 7=M03; 8=Milichius Pi; 9=H02; 10=Arago Beta; and 11=Arago Alpha

7. Discussion:

The correspondence in results of dome height and diameter between the present study using Carlotto's algorithm in EXCEL and previous measurements of these domes by the GLR group is encouraging considering the low profile of these structures which are being viewed from a distance approaching 400,000 km. The present study show dome heights that are slightly less (an average of 9% less for the eleven domes studied) than the heights measured in

previous studies by GLR summarized by Wöhler et al. (2006). These studies utilized a lunar Lambertian algorithm. The underestimation observed in the present study was an expected result as the Carlotto approximation which tends to underestimate the slope of lunar features (and therefore feature heights) by a small amount. The approximation provided by this simple Lambertian method is less accurate when features under study are viewed from an increasingly oblique angle (i.e. they are positioned closed to the lunar limb). For example, this is evident in height approximations obtained for the dome Y01 near Yerkes (Fig. 6). The Carlotto algorithm, however, is simple to execute and may still be useful to amateurs desiring a flexible, transparent, rapid and inexpensive means of making photoclinometric measurements of lunar domes as long as its limitations are kept in mind. For those having some experience with Visual Basic Application (VBA) programming, it would not be too difficult to achieve a greater degree of automation by inserting a subroutine to move data columns between worksheets into the existing macro script I have provided. Future studies might include a detailed analysis of the effect of increasing lunar longitude on dome height measurement using the Carlotto algorithm.

Acknowledgements:

The author wishes to thank Christian Wöhler and Raffaelo Lena of the GLR group for their assistance and encouragement without which it would not have been possible to pursue this project. He also wishes to thank the GLR group for making images of the lunar domes used in this paper available and in particular to thank the following GLR imagers for the excellent quality of their lunarphotographs: Christian Fattinnanzi, Paolo Lazzarotti, Jim Philips, Zac Pujic, and Michael Wirths.

APPENDIX 1: STUDIES OF TEN ADDITIONAL DOMES

STUDY #1: Dome H01 near Hortensius

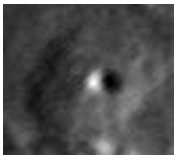

Fig.7: H01 dome.

Image by Mike Wirths (GLR Group)

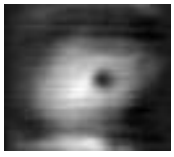

Fig.8: H01 dome, digital elevation map:

Height at pixel = 212((Pv/50)-3) meters/pixel.*

Longitude -28.41 Latitude 7.18; Zenith Angle -87 degrees; Resolution 212 meters/pixel; curvature corrected

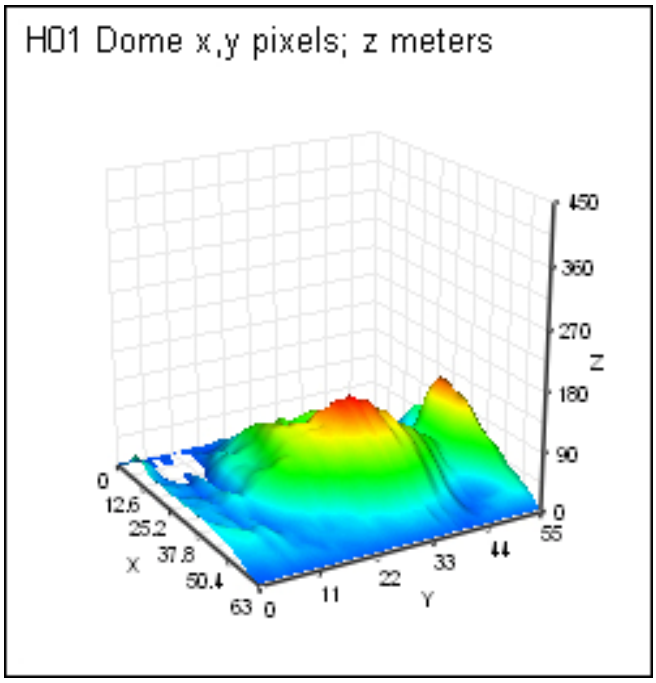

Fig.9: H01 dome, 3D plot.

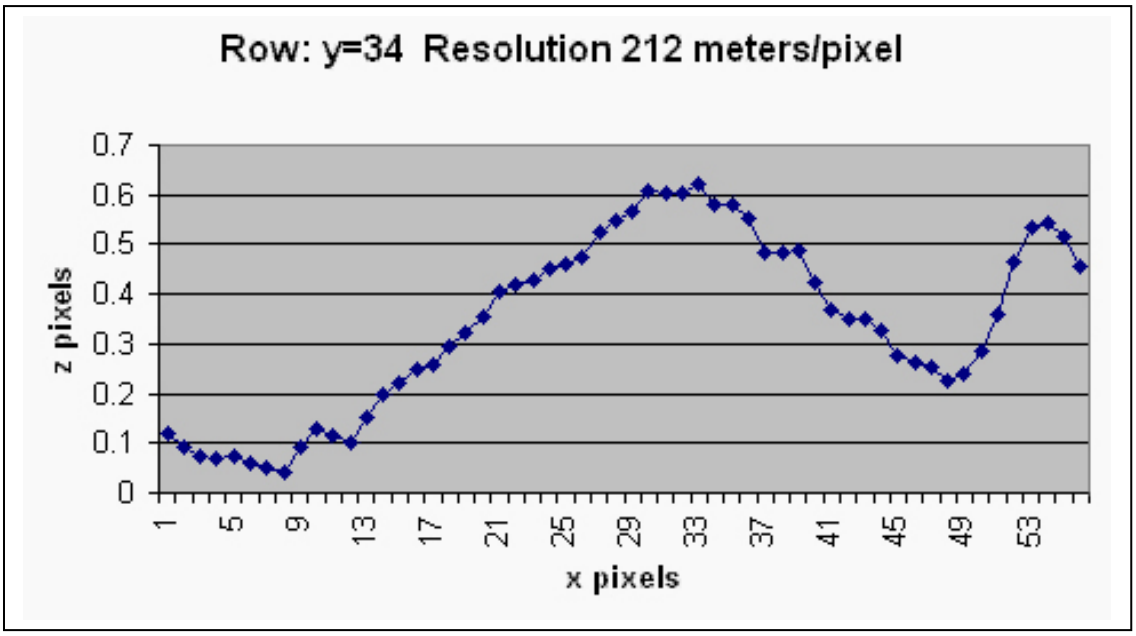

Fig.10: H01 dome, Excel plot.

The dome height corrected for lunar curvature is 117.8 meters +/- 11.78 meters (the estimated camera gamma calibration error).

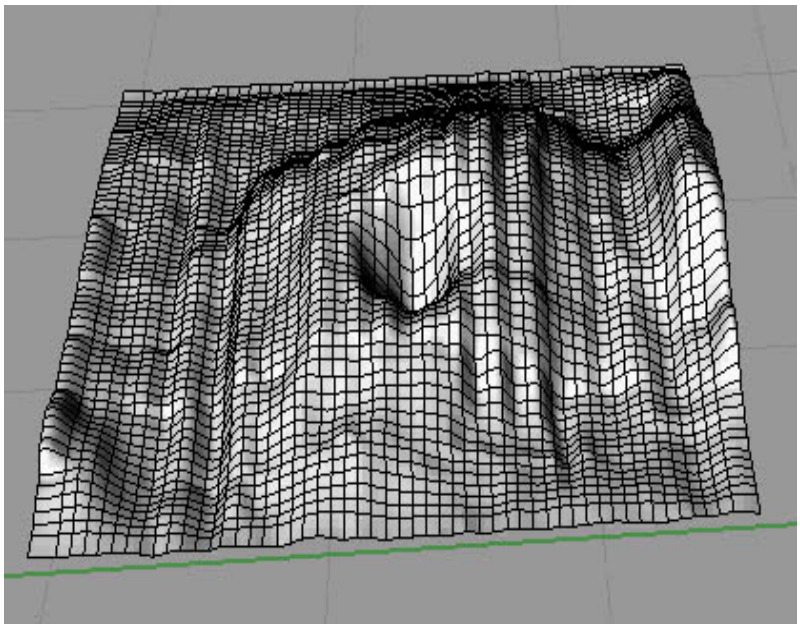

Fig.11: H01 dome, topographic plot of digital elevation map in Rhino 3.0 with Height Scale 3.0x.

STUDY #2: Arago Alpha Dome:

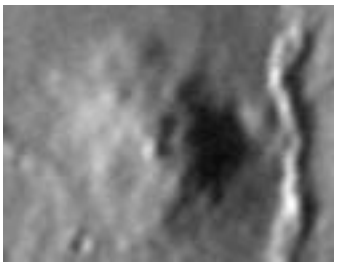

Fig.12:Arago alpha dome.

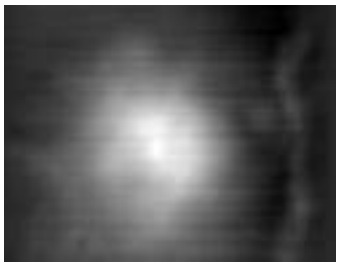

Fig.13:Arago alpha dome, digital elevation map.

Height at pixel = 321((Pv/50)-3) meters/pixel.*

Image by Paolo Lazzarotti (GLR Group)

21.7 longitude; 7.56 latitude; 87.03 Zenith Angle; Resolution 321 meters/pixel; curvature corrected

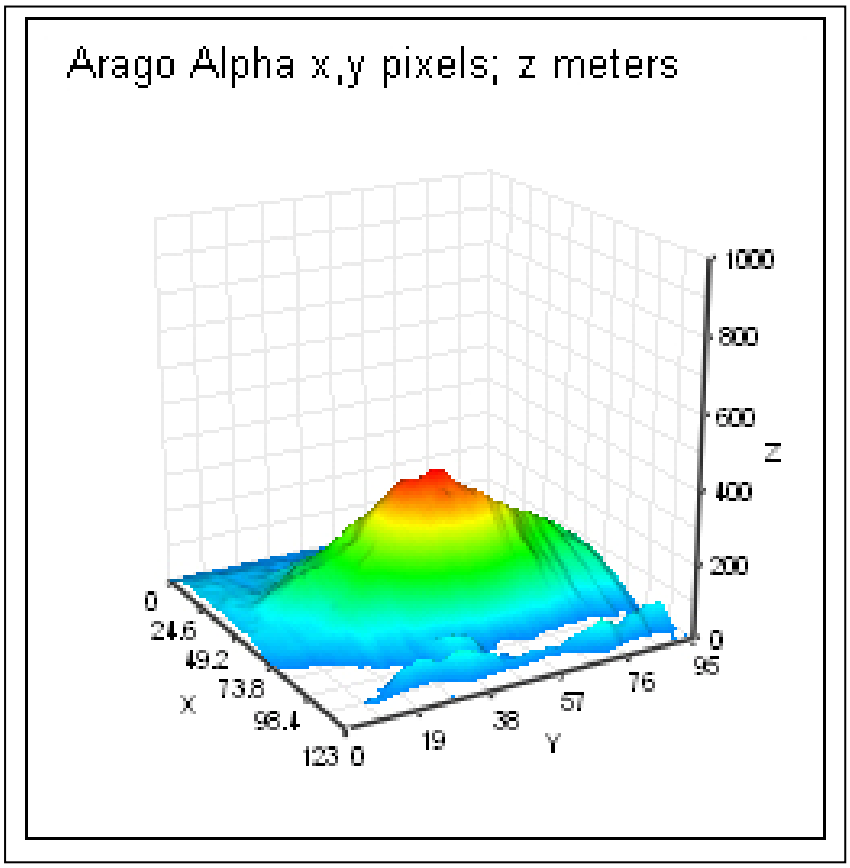

Fig.14:Arago alpha dome, 3D plot.

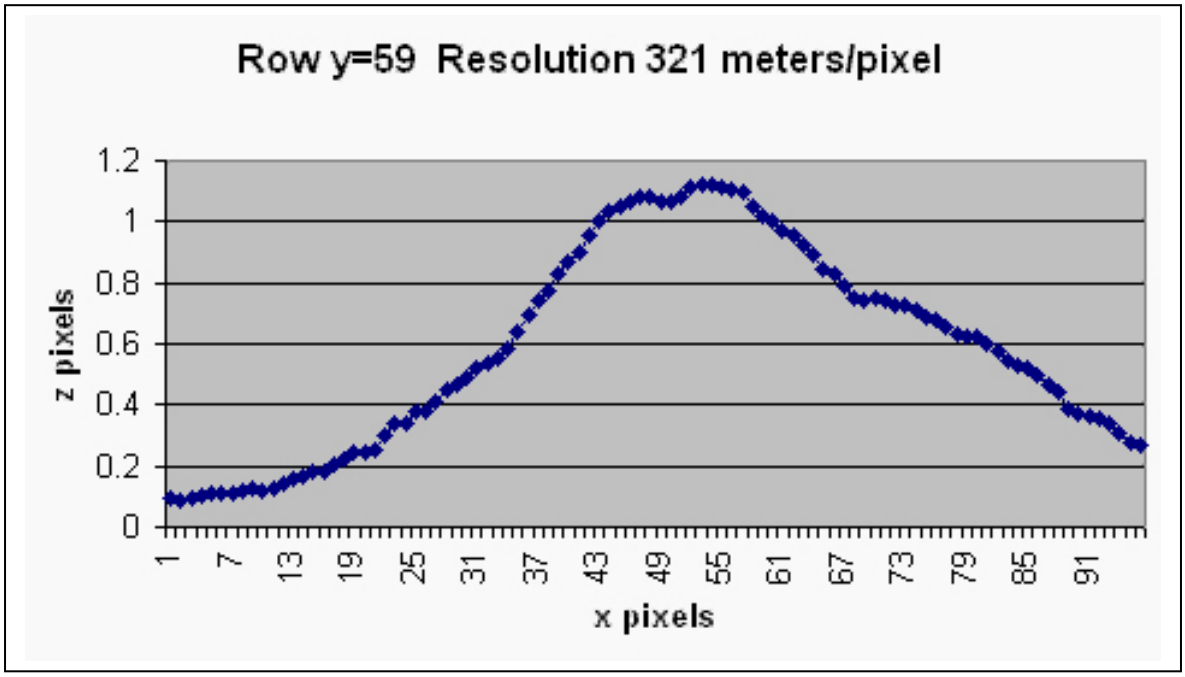

Fig.15:Arago alpha dome, Excel plot.

The corrected dome height is 282 meters +/- 28.2.

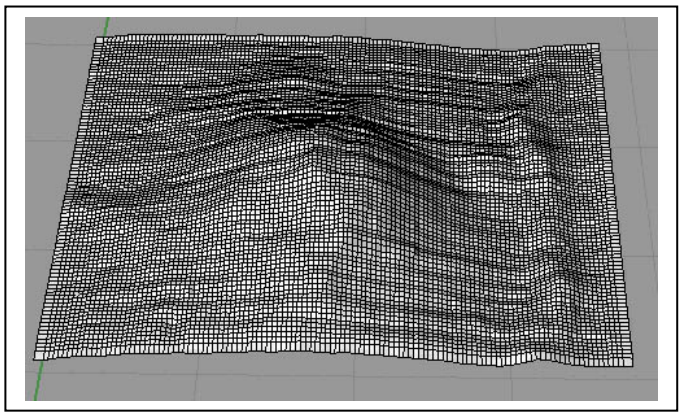

Fig.16:Arago alpha dome, topographic plot of digital elevation map in Rhino 3.0 with Height Scale 3.0x.

Study #3: Dome H07 near Hortensius E

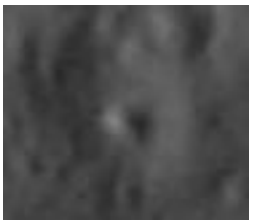

Fig.17:H07 dome.

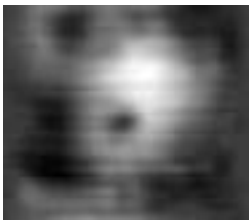

Fig.18:H07 dome, digital elevation map. Greyscale subtraction for overlying shadow: 20 units. Height at pixel = 158((Pv/50)-3)meters/pixel*

Image by Zac Pujic (GLR Group)

Longitude -25.17; Latitude 6.07; Zenith Angle -86.47; Resolution 158 meters/pixel

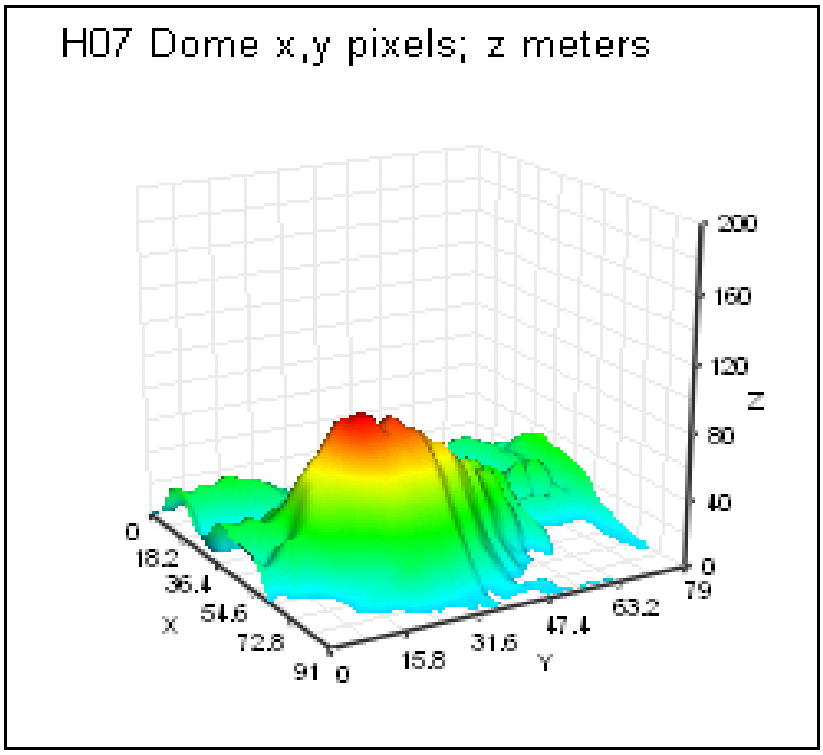

Fig19: H07 dome, 3D plot.

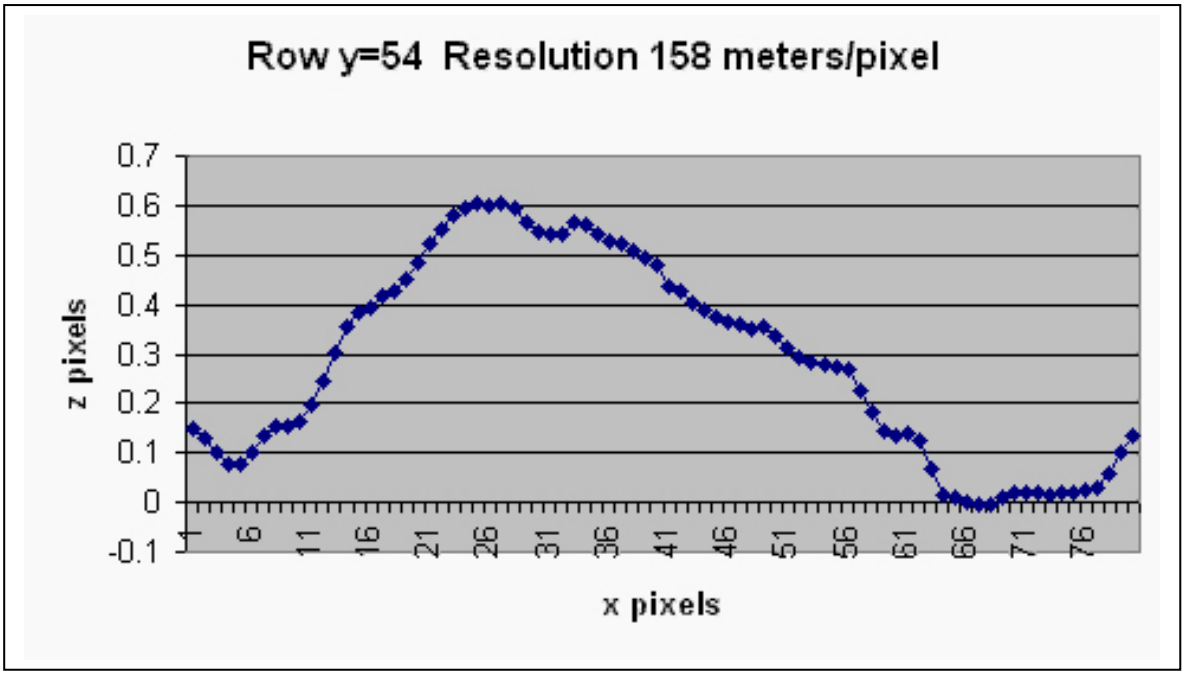

Fig.20: H07 dome, Excel plot.

Dome height after subtraction of curvature 62.4 meters +/- 6.24 – Dome diameter: 9.8 km

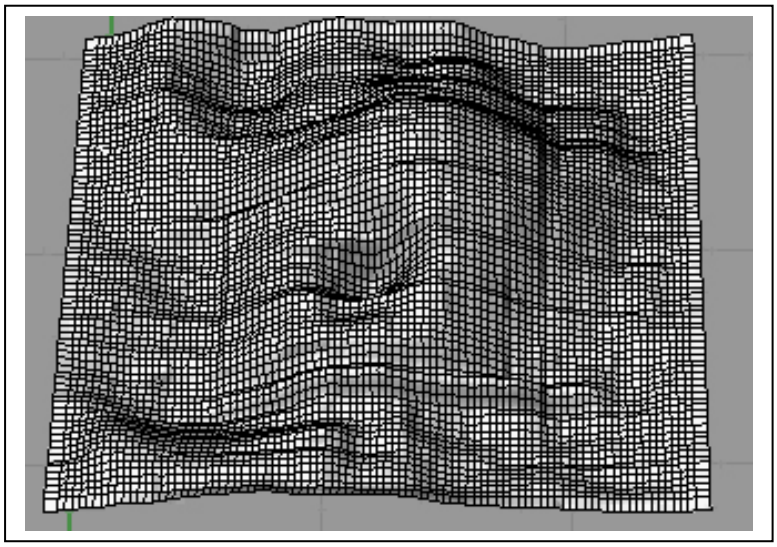

Fig.21: H07 dome, topographic plot of digital elevation map in Rhino 3.0 with Height Scale 3.0x.

Study #4: Cauchy Tau Dome

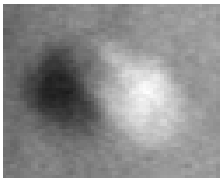

Fig.22: Cauchy Tau dome.

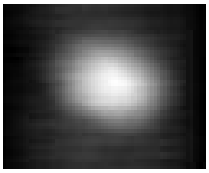

Fig.23: Cauchy Tau dome, digital elevation map.

Height at pixel = 365((Pv/50)-3) meters/pixel.*

Image by Paulo Lazzarotti (GLR Group)

Longitude 36.73; Latitude 7.58; Zenith Angle -87.39; Resolution 365 meters/pixel

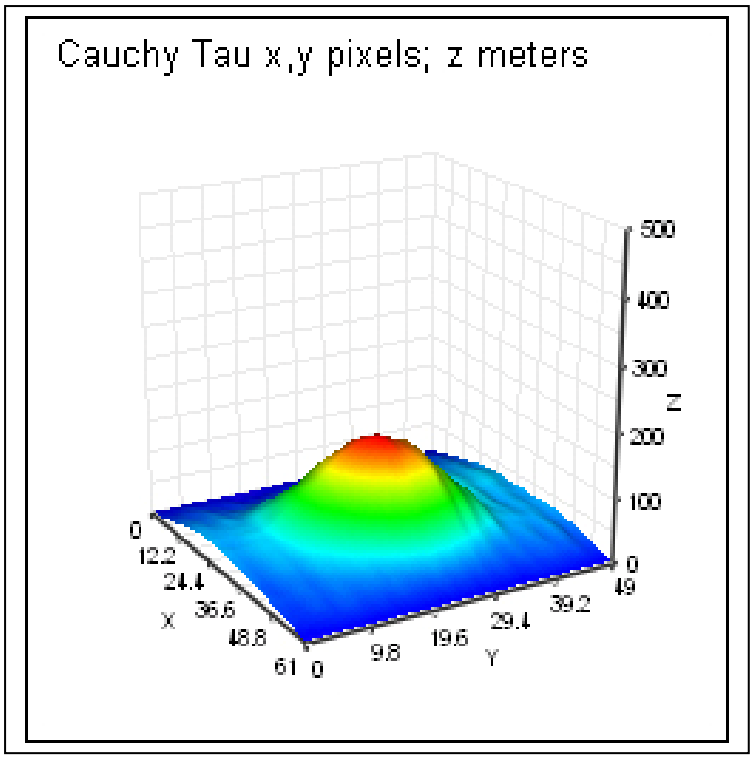

Fig.24: Cauchy Tai, 3D plot.

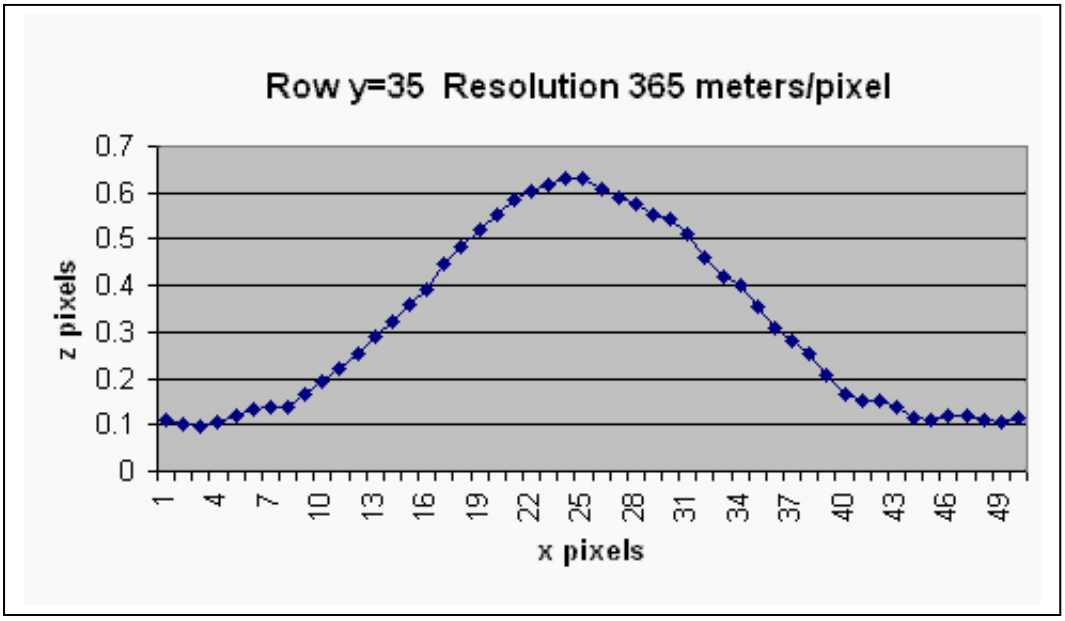

Fig.25: Cauchy Tau dome, Excel plot.

Dome Height after correcting for curvature: 174.1 meters – Dome Diameter: 15.0 km

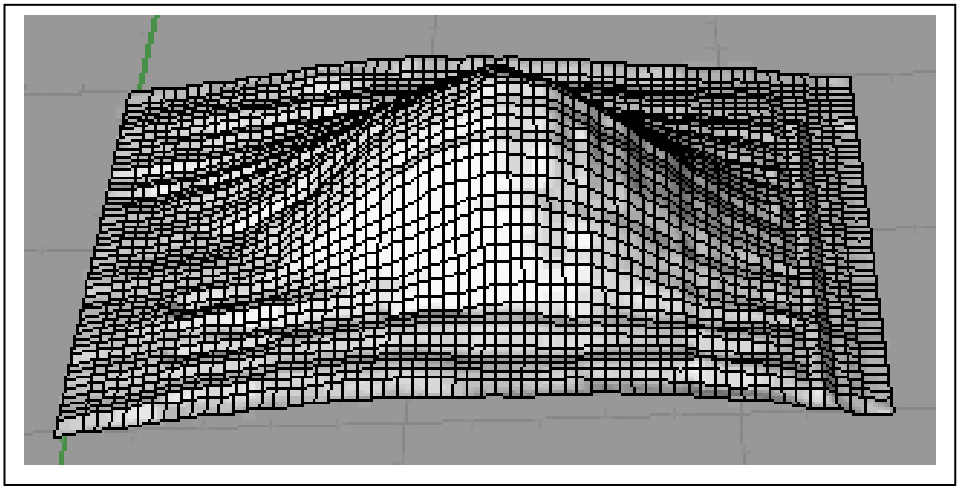

Fig.26: Cauchy Tau dome, topographic plot of digital elevation map in Rhino 3.0 with Height Scale 3.0x.

Study #5: Milichius Pi dome (M12)

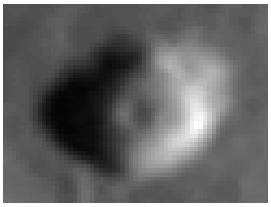

Fig.27: Milichius Pi dome (M12).

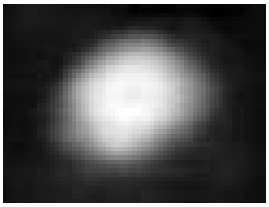

Fig.28: Milichius Pi dome (M12), digital elevation map.

Height at pixel = 296((Pv/50)-3) meters/pixel.*

Image by: Jim Philips

Longitude -31.2; Latitude 10.08; Zenith Angle -87.29; Resolution 296 meters/pixel

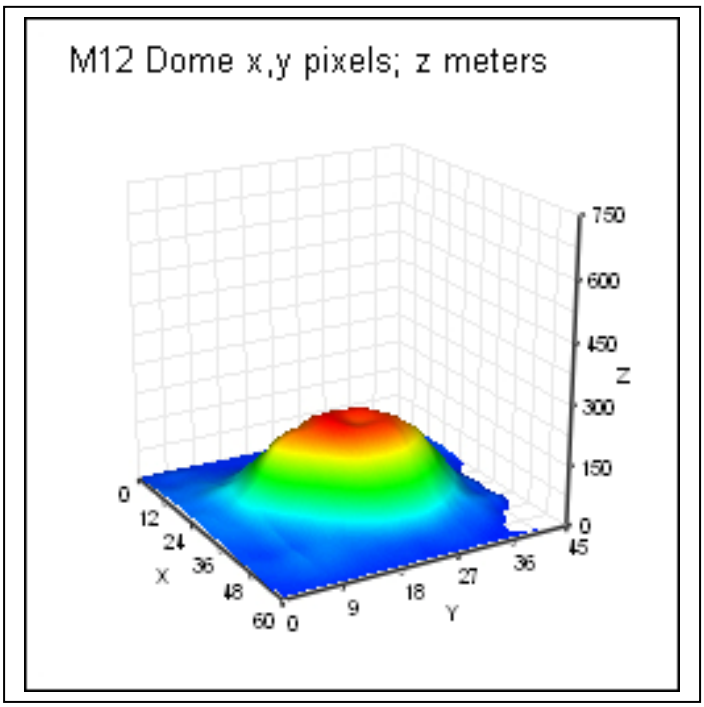

Fig.29: Milichius Pi dome (M12), 3D plot.

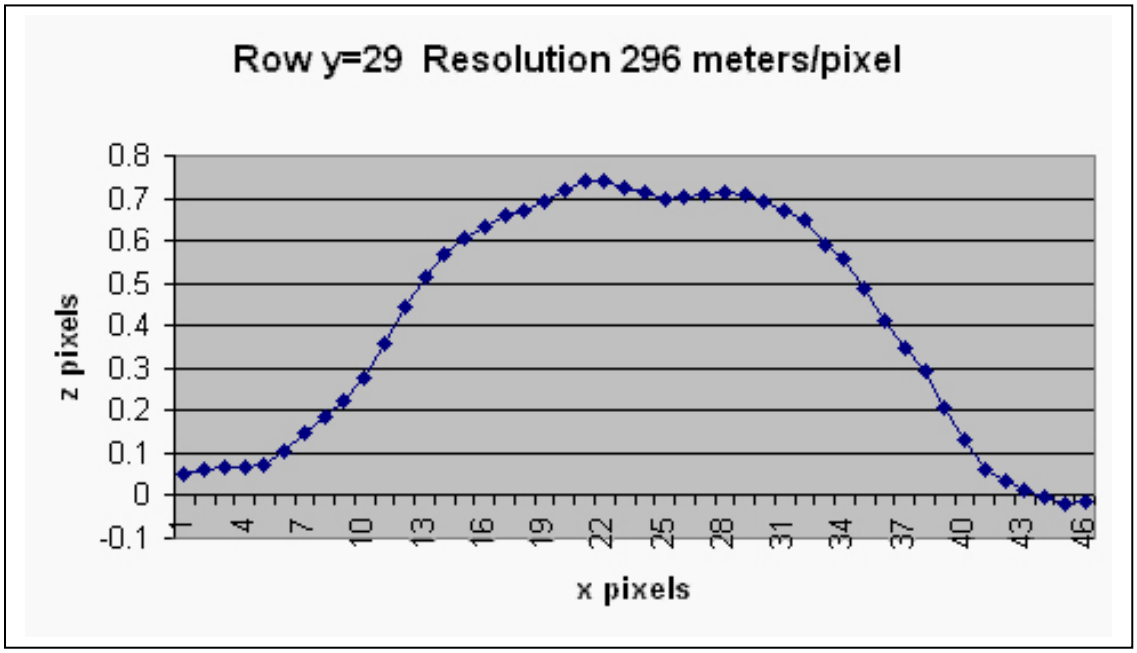

Fig.30: Milichius Pi dome (M12), Excel plot.

Dome height corrected for lunar curvature: 214.5 meters +/- 21 meters.

Dome Diameter: 11.85 km

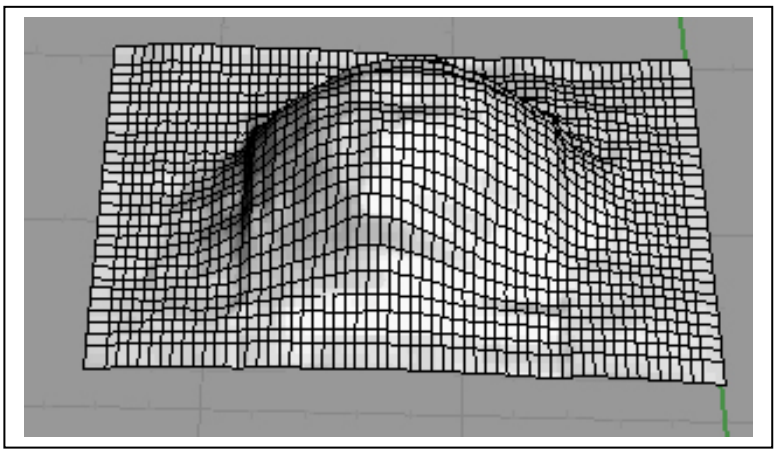

Fig.31: Milichius Pi dome (M12), topographic plot of digital elevation map in Rhino 3.0 with Height Scale 3.0x

Study #6: Arago Beta (ao3)

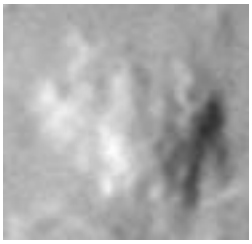

Fig.32: Arago Beta dome.

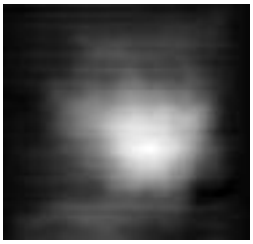

Fig.33:Arago Beta dome (A03), digital elevation map.

Height at pixel = 321((Pv/50)-3) meters/pixel.*

Image by: Paolo Lazzarotti (GLR Group)

Longitude 20.07; Latitude 6.24; Zenith Angle 85.36; Resolution 321 meters/pixel

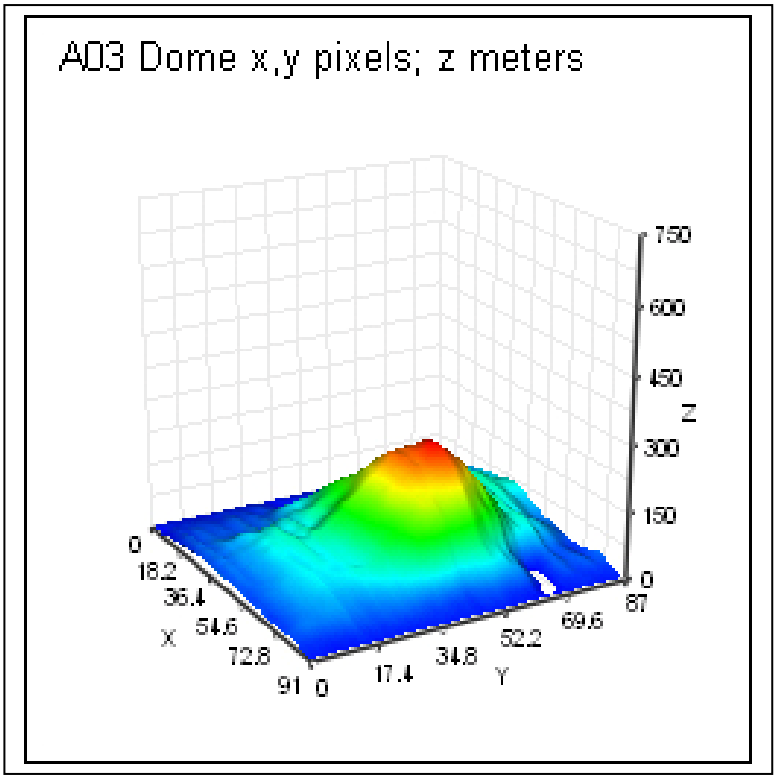

Fig.34: Arago Beta dome (A03), 3D plot

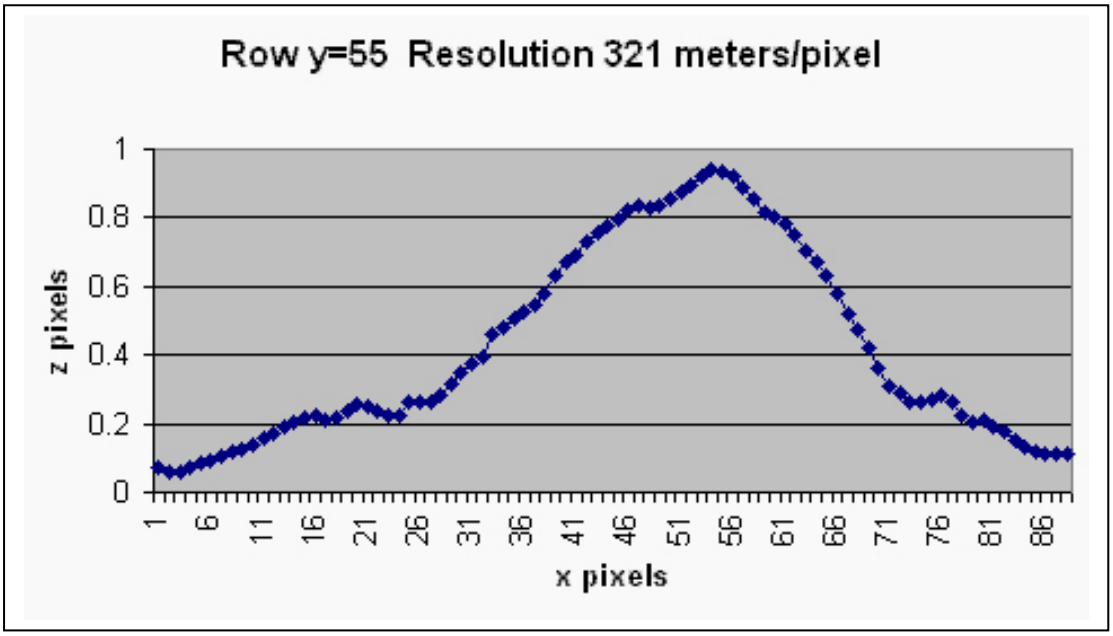

Fig.35: Arago Beta dome (A03), Excel plot.

Dome Height Corrected for Curvature Contribution: 264.1 meters

Dome height 16 km

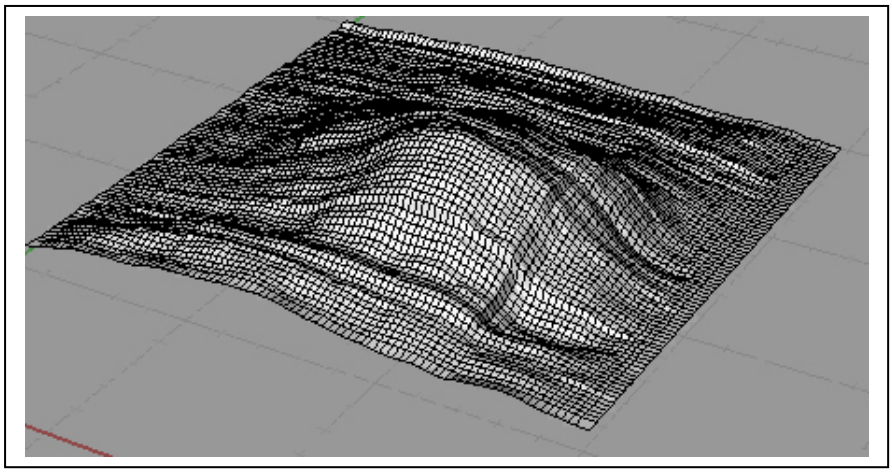

Fig.36: Arago Beta dome (A03), topographic plot of digital elevation map in Rhino 3.0 with Height Scale 3.0x

Study #7: Dome H02

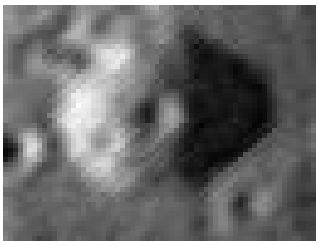

Figure 37:H02 dome.

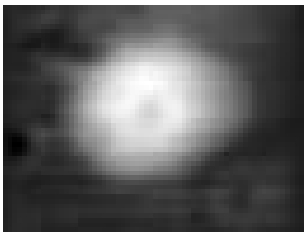

Figure 38: H02 dome, digital elevation map.

Height at pixel =212((Pv/50)-3) meters/pixel.*

Imager: Mike Wirths

Longitude -28.01; Latitude 7.12; Zenith angle -86.6; Resolution 212 meters/pixel

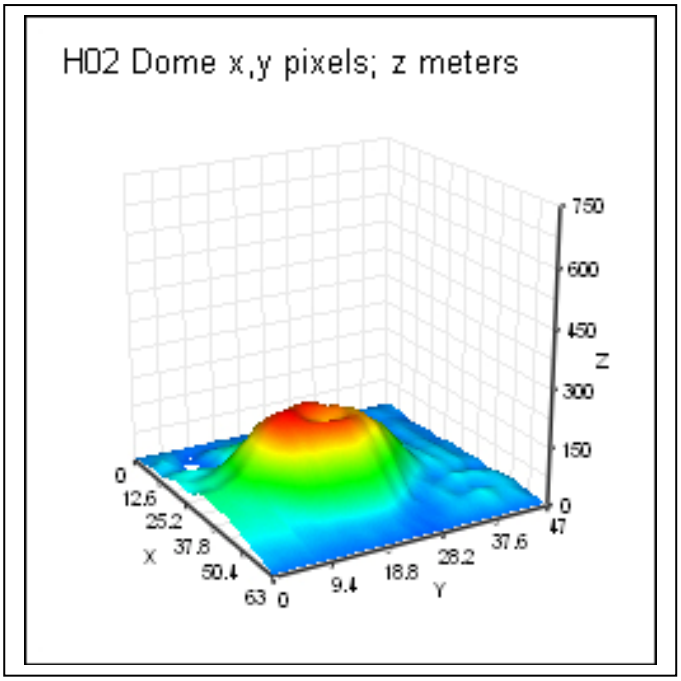

Fig.39: H02 dome, 3D plot.

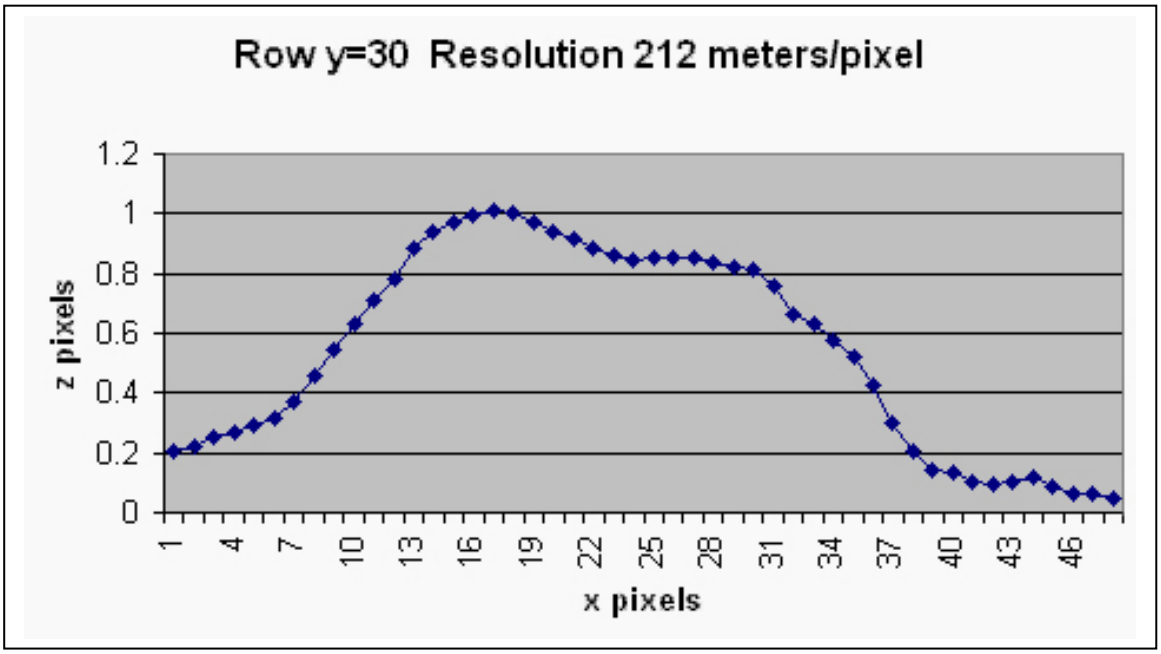

Fig.40: H02 dome, Excel plot.

Height of dome correcting for curvature contribution: 201.1 meters +/- 20.1

Dome diameter: 7.2 km +/- 0.72

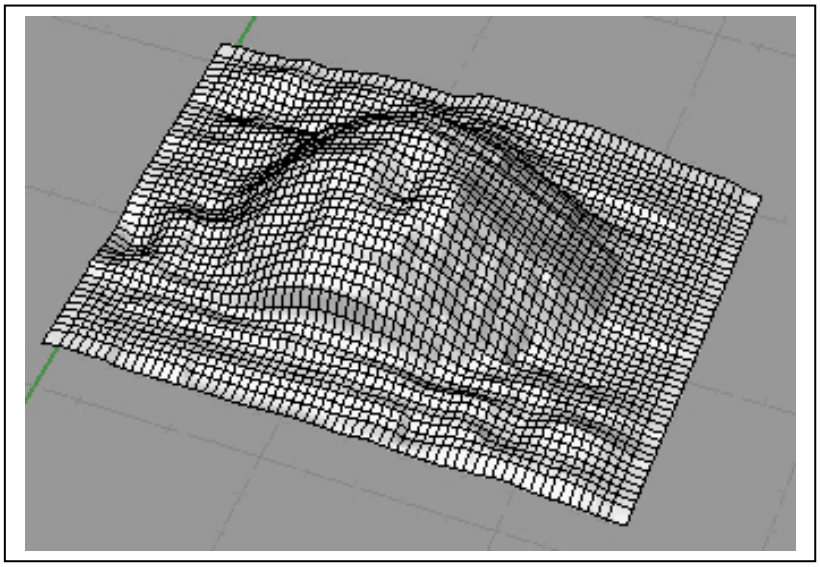

Fig.41: H02 dome, topographic plot of digital elevation map in Rhino 3.0 with Height Scale 3.0x

Study #8: Dome m03 near Milichius

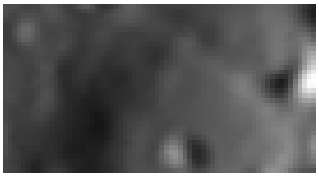

Fig.42: M03 dome.

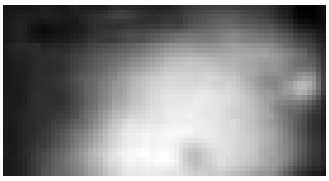

Fig.43: M03 dome, digital elevation map.

Height at pixel=296((Pv/50)-3) meters/pixel.*

Imager: Jim Philips (GLR Group)

Longitude -30.43; Latitude 13.78; Zenith angle -86.67; Resolution 296 meters/pixel

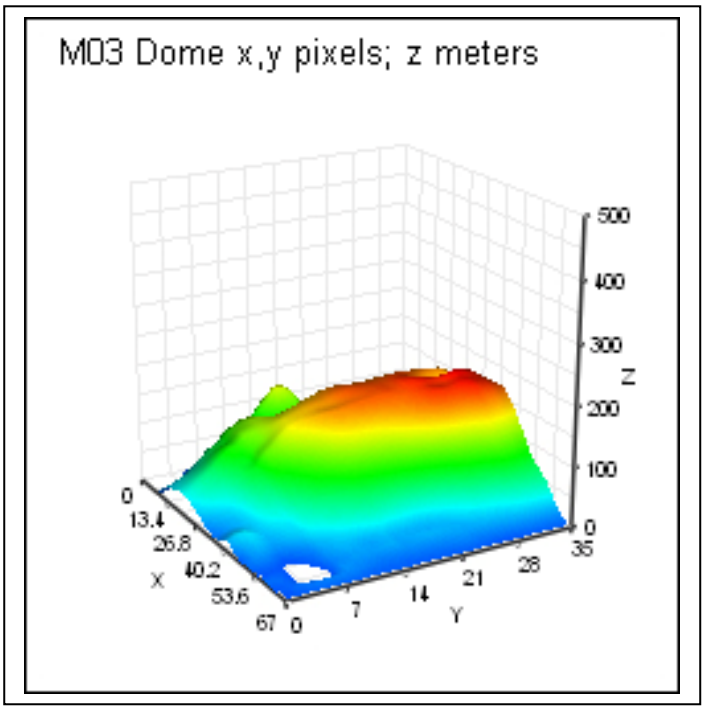

Fig.44: M03 dome, 3D plot.

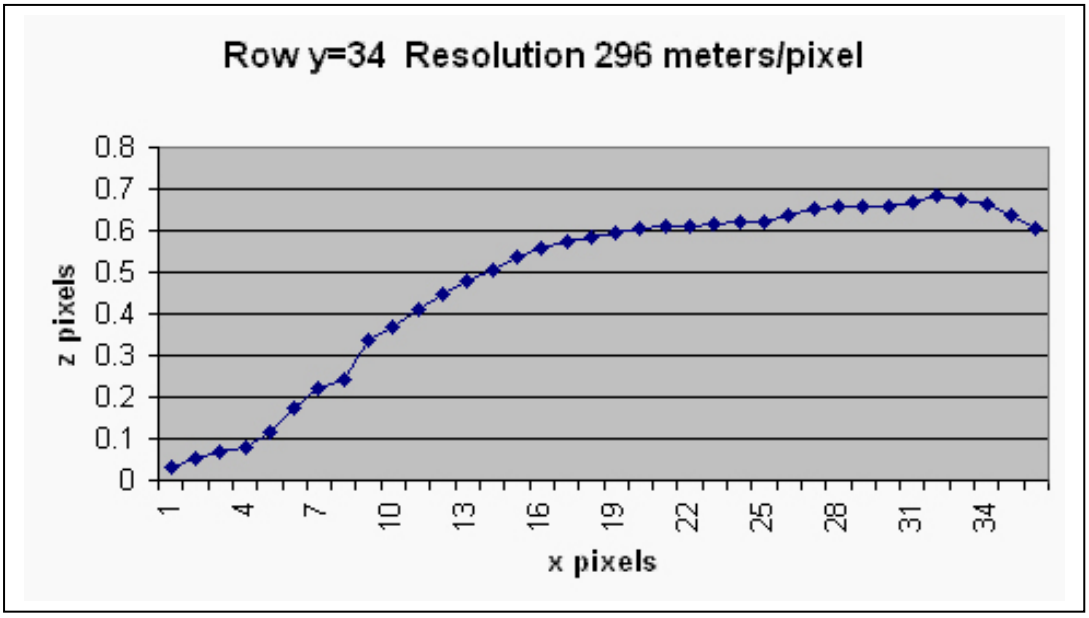

Fig.45: M03 dome, Excel plot.

Dome height corrected for lunar curvature: 189.52 meters

Dome diameter: 12.43 km

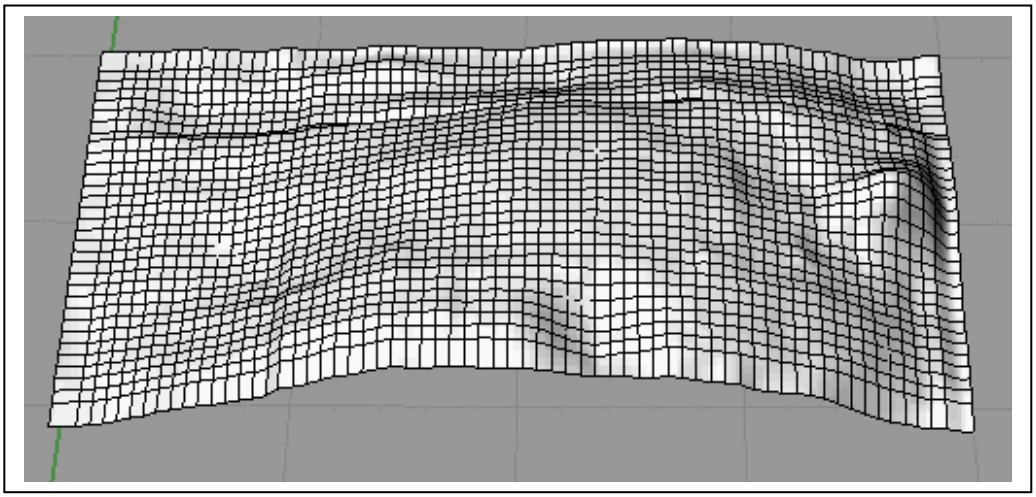

Fig.46: M03 dome, topographic plot of digital elevation map in Rhino 3.0 with Height Scale 3.0x

Study #9: Dome Y01 near Yerkes

Fig.47: Y01 dome.

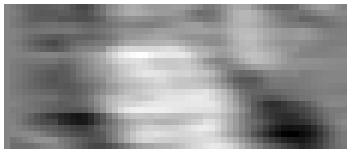

Fig.48: Y01 dome, digital elevation map.

Height at pixel =280((Pv/50)-3) meters/pixel.*

Imager: Cristian Fattinnanzi (GLR Group)

Longitude 49.96; Latitude 14.82; Zenith angle 79.09; Resolution 280 meters/pixel

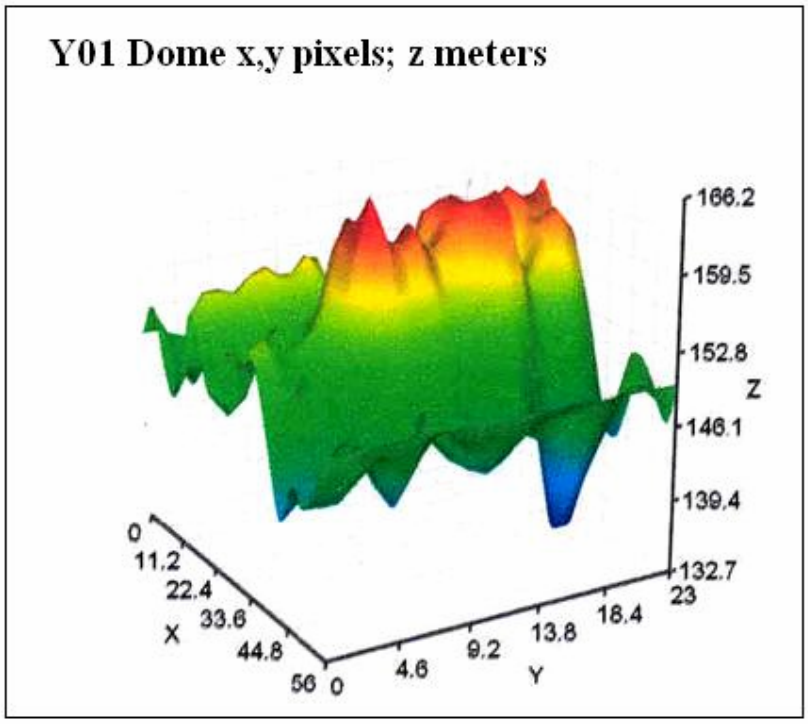

Fig.49: Y01 dome, 3D plot.

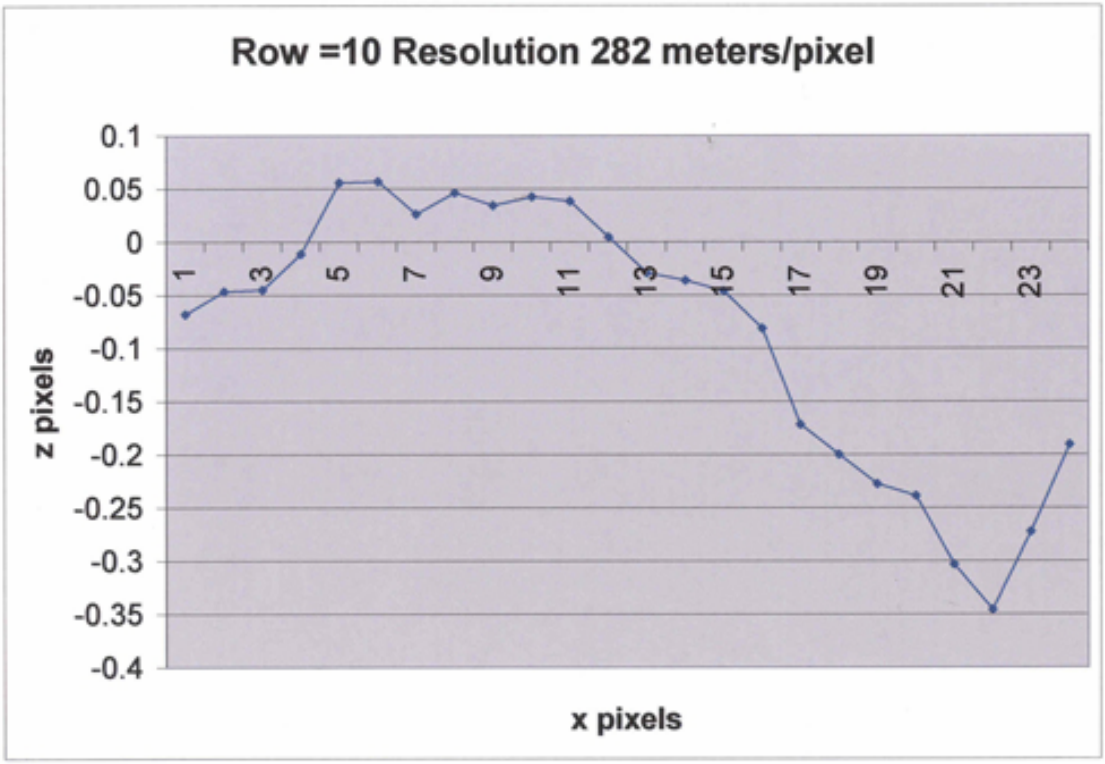

Fig.50: Y01 dome, Excel plot.

Dome height corrected for curvature contribution: 109.22 met

Diameter of higher peak of dome: 12.6 km

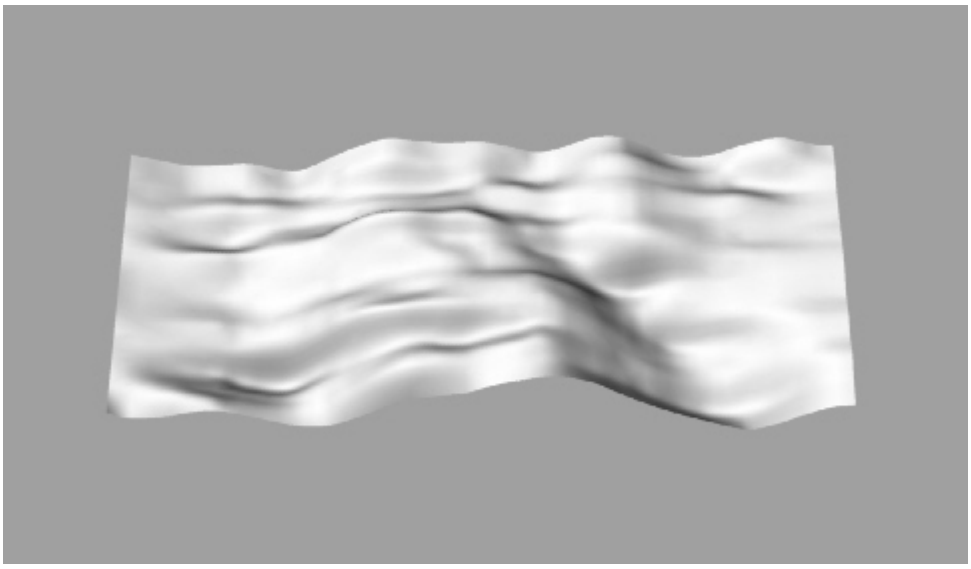

Fig.51: Y01 dome, topographic plot of digital elevation map in Rhino 3.0 with Height Scale 3.0x

Study #10: Dome A01 near Arago

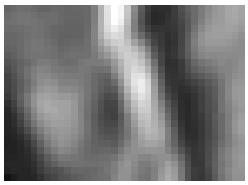

Fig.52: A01 dome.

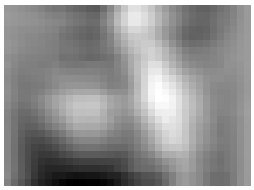

Fig.53: A01 dome, digital elevation map.

Height at pixel =321((Pv/50)-3) meters/pixel.*

Image by Jim Philips (GLR Group)

Longitude 21.96 Latitude 7.66; Zenith Angle 87.32; Resolution 321 meters/pixel

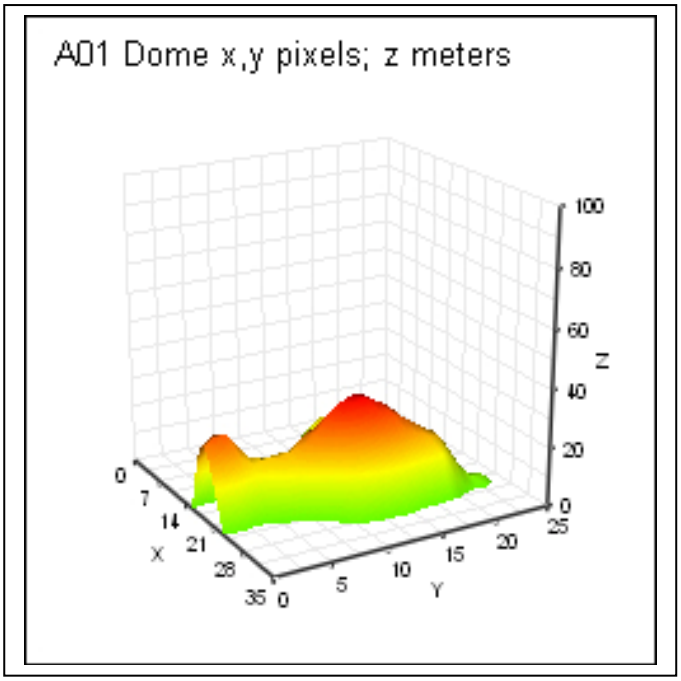

Fig.54: A01 dome, 3D plot.

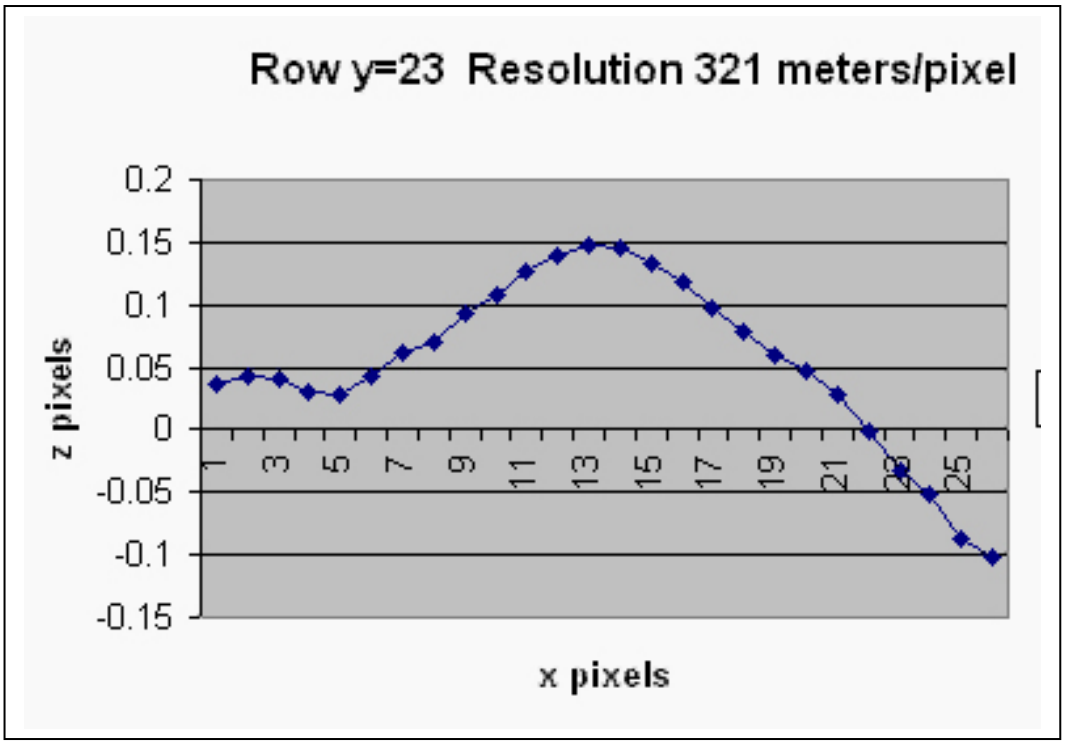

Fig.55: A01 dome, Excel plot.

Dome height corrected for lunar curvature: 35.78

Dome diameter: 5.46 km

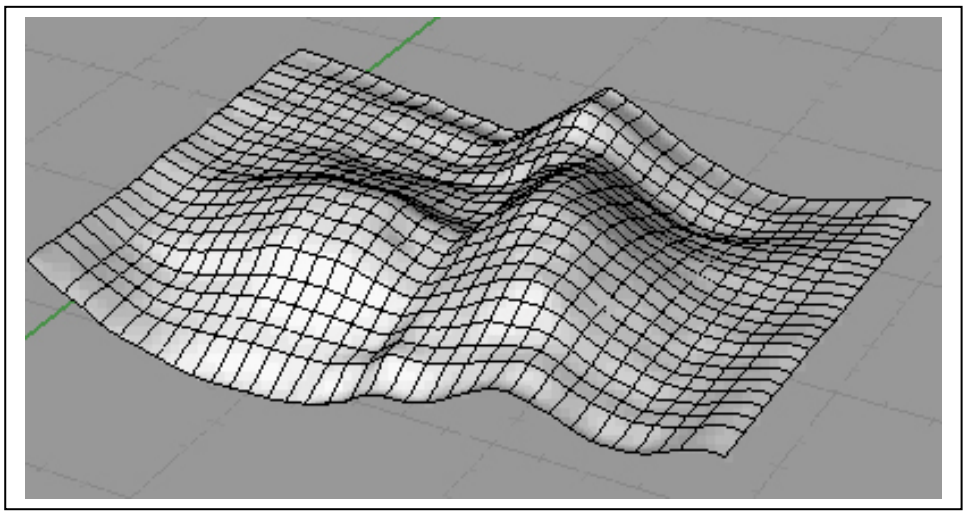

Fig.56: A01 dome, topographic plot of digital elevation map in Rhino 3.0 with Height Scale 3.0x

Appendix 2: EXCEL Tutorial

The image data (.txt) file created using Image Magick is opened in EXCEL choosing the delimited option and with import starting at row 2 in the dialog box of the EXCEL txt Import Wizard. Delimiters are set as comma, semicolon, and colon. The imported is "cleaned up" on the EXCEL spreadsheet by leaving only three columns of data: the x values (i.e. the column numbers), the y values (or row numbers) and the z values (or pixel grey values). These are located on the first three data columns of the spreadsheet (A, B and C). The data is grouped in data blocks consisting of consecutive data elements for each row in the image beginning at row 0. The first step in processing is to determine the average pixel value for the first image row, which consists of the data block corresponding to y values equal to zero and the associated x and z values. This is done by starting at cell C1 and dragging down with the left clicked cursor from the midportion of the cell until all data elements for row 0 are highlighted. Then the fx button is selected from the toolbar and AVERAGE is chosen as the function from the dialog box. The range for row 0 is entered (i.e. as C1:Cn where n is the row number in EXCEL of the last data element in column C for the data block of all zero y values. The average pixel value is then read and manually entered into cell I1. Next cells I1 to In are highlighted by dragging the left clicked cursor and the Fill/Series/Columns/Linear/Step Value 0 option is selected from the Edit menu.

This yields a data colum at I on the spreadsheet of the same length as the data block for row 0 whose cells all contain the same number (i.e. the average pixel grey value for the row). This process is now automated by creating a keyboard Macro. A Macro is a subroutine that simply remembers a series of recorded keystrokes and clicked cursor movements. To do this, the Macro/Record Macro option is selected from the Tools menu. A name for the macro is selected (i.e. AvgPV) and a keyboard call for the macro is assigned as <Cntrl> d. Each step in the process of creating column F defined above is then repeated and the Stop Recording option is selected from the Tools Menu.Calculate the tangent of the phase angle in degrees for the image. Select cell J1 with the cursor. Type the following into the cell: =(C1-I1)/(I1*tangent of the phase angle in degrees) and hit Enter. Select cell J1 with the cursor and move the cursor to the lower right hand corner of the cell. Now left click and drag downwards to position Jn. Note that when you left click and drag the lower right hand border of a cell, a + sign appears on the spreadsheet at that position. The resulting data column represents the Carlotto Lambertian transform function applied to the greyscale values of the image. This process is now automated by creating a keyboard Macro in the manner described above. The Macro is named Transform and assigned to the keyboard call <Cntrl> e.Select cell K1 by cursor click and type, =J1, then hit the enter key. Now select cell K2 by cursor click and type, =K1 + J2, then hit the enter key. Next position the cursor at the lower right hand corner of cell K2 and left click and drag the cursor downward to position Kn. Note that when you left click and drag the lower right hand border of a cell, a + sign appears on the spreadsheet at that position. The numbers in column K represent a rolling summation of the transform function defined in column J. This process is now automated by creating a keyboard Macro in the manner described above. The Macro is named Summation and assigned to the keyboard call ,Cntrl. f. Now select cell L1 and type =(K1+3)*50 then hit the enter key. Left click the lower right hand corner of the cell (again, a + sign will appear on the spreadsheet) and drag downward to position Ln. The resulting column represents greyscale values of a heightmap (i.e. digital elevation map) of the original image. The parameters 3 and 50 are somewhat arbitrary and are chosen to bring the greyscale values into the 0 to 255 range for most lunar images taken under oblique lighting. The process is now automated by creating a Macro as discussed above. The Macro is named Greyscale and is assigned to keyboard call <Cntrl> g.

Next two additional spreadsheets are created within the same workbook. The first is named TransSum and the second Greyscale. Column K is copied to column A of the spreadsheet TransSum using the PasteSpecial option under the edit menu and selecting Values from the dialog box. Column L is copied to column A of the spreadsheet Greyscale in the same manner. Finally, returning to the original spreadsheet, all data for EXCEL rows corresponding to y values equal to zero (i.e. the entire data block for y=0) is deleted from the spreadsheet and remaining data columns are shifted up to the top of the spreadsheet. This includes deleting not only data columns A, B and C but also data columns I, J, K and L for the first data block corresponding to y=0. After this process, the data block at the top of the spreadsheet corresponds to x, y and z values corresponding to the data block y=1. If desired, additional Macros can be defined to perform these copy, paste and block delete functions to save time. An example of the coding for these Macros has been included in Appendix 3.This completes the first iteration (i.e. the processing of data for row 0 of the image). To perform the next iteration keyboard Macros are sequentially called up by entering their call functions. Pressing <Cntrl> d re-creates column I which now holds average greyscale values for the data block y=1. Pressing <Cntrl> e re-creates column J which now holds the Carlotto Lambertian transform function values for data block y=1. Pressing <Cntrl> f re-creates column K which holds the rolling summation of the transform values for data block y=1. Pressing <Cntrl> g re-creates column L which holds the digital elevation map greyscale values corresponding to the original image for data block y=1. Column K is copied to Column B of spreadsheet TransSum. Column L is copied to Column B of spreadsheet Greyscale. The data block corresponding to y=1 (i.e. columns A, B, C, I, J, K and L for y=1) are then deleted and the remaining cells are up shifted to the top of the spreasheet. This now brings the data block corresponding to y=2 to the top of the spreadsheet. Subsequent iterations are performed in exactly the same manner until all data blocks have been processed and processed data has been sequentially added to the next available column on spreadsheets TransSum and Greyscale. When the process is completed, data in any row of TransSum can be graphed to obtain A height profile for that row (remember that height in meters equals the cell value for that point multiplied by the pixel resolution of the original image). In addition, the Greyscale spreadsheet data can be exported as a tab delimited file which is then imported as a text image file into the program ImageJ and used to generate a picture

picture image of the digital elevation map that was generated from the original image. Experienced EXCEL users may find it desirable to fully automate the process of the generation of data in speadsheets TransSum and Greyscale by programming directly in Visual Basic for Applications (VBA) within EXCEL. Although not very complicated, this does require programming experience and was beyond the scope of the present paper. However, most amateur astronomers including those with little or no prior EXCEL experience should be able to create functional Macros to create the spreadsheet data via the process outlined above with little difficulty.

Appendix 3: Visual Basic Script for Macros

Used in Example of Cauchy Omega Dome

1. Macro Script to Determine Average Pixel Values for a Row

```
Sub AvgPV()
'
' AvgPV Macro
' Macro recorded 3/10/2006 by Richard Evans
'
' Keyboard Shortcut: Ctrl+e
'
    Range("I1").Select
    ActiveWindow.SmallScroll Down:=43
    ActiveWindow.ScrollRow = 1
    ActiveCell.FormulaR1C1 = "=AVERAGE(RC[-6]:R[52]C[-6])"
    Range("I1").Select
```

```
    Selection.AutoFill Destination:=Range("I1:I53"), Type:=xlFillDefault
    Range("I1:I53").Select
    ActiveWindow.ScrollRow = 1
    Range("J1").Select
End Sub
```

2. Macro to Apply Carloto's Lambertian Transform to a Row

```
Sub Transform()
'
' Transform Macro
' Macro recorded 3/5/2006 by Richard Evans
'
' Keyboard Shortcut: Ctrl+f
'
    Range("J1").Select
    ActiveCell.FormulaR1C1 = "=(RC[-7]-RC[-1])/(RC[-1]*13.65)"
    Range("J1").Select
    Selection.AutoFill Destination:=Range("J1:J53"), Type:=xlFillDefault
    Range("J1:J53").Select
    ActiveWindow.ScrollRow = 1
    Range("K1").Select
End Sub
Sub Summation()
```

```
 Sub Summnation ()
 ' Summation Macro
 ' Macro recorded 3/5/2006 by Richard Evans
 '
 ' Keyboard Shortcut: Ctrl+g
 '
  ActiveCell.FormulaR1C1 = "=RC[-1]"
  Range("K2").Select
  ActiveCell.FormulaR1C1 = "=R[-1]C+RC[-1]"
  Range("K2").Select
  Selection.AutoFill Destination:=Range("K2:K53"), Type:=xlFillDefault
  Range("K2:K53").Select
  ActiveWindow.ScrollRow = 1
  Range("L1").Select
End Sub
```

3. Macro to Iteratively Sum Transform Values Along a Row

```
Sub Summation()
'
' Summation Macro
' Macro recorded 3/5/2006 by Richard Evans
'
' Keyboard Shortcut: Ctrl+g
'
```

```
ActiveCell.FormulaR1C1 = "=RC[-1]"
  Range("K2").Select
  ActiveCell.FormulaR1C1 = "=R[-1]C+RC[-1]"
  Range("K2").Select
  Selection.AutoFill Destination:=Range("K2:K53"), Type:=xlFillDefault
  Range("K2:K53").Select
  ActiveWindow.ScrollRow = 1
  Range("L1").Select
End Sub
```

4. Macro to Copy a Column of Iteratively Summed Transform Values

```
Sub CopySum()
'
' CopySum Macro
' Macro recorded 3/5/2006 by Richard Evans
'
' Keyboard Shortcut: Ctrl+h
'
    Range("K1:K53").Select
    Selection.Copy
    ActiveWindow.ScrollRow = 1
    Range("L1").Select
End Sub
```

5. Macro to Convert Iteratively Summed Transform Values to Greyscale DEM

```
Sub Greyscale()
'
' Greyscale Macro
' Macro recorded 3/5/2006 by Richard Evans
'
' Keyboard Shortcut: Ctrl+i
' Range("L1").Select
    Application.CutCopyMode = False
    ActiveCell.FormulaR1C1 = "=(RC[-1]+3)*50"
    Range("L1").Select
    Selection.AutoFill Destination:=Range("L1:L53"), Type:=xlFillDefault
    Range("L1:L53").Select
    ActiveWindow.ScrollRow = 1
    Range("M1").Select
End Sub
```

6. Macro to Copy Column of Greyscale DEM Values

```
Sub CopyGreyscale()
'
' CopyGreyscale Macro
' Macro recorded 3/5/2006 by Richard Evans
'
```

```
' Keyboard Shortcut: Ctrl+j
'
    Range("L1:L53").Select
    Selection.Copy
    ActiveWindow.ScrollRow = 1
    Range("M1").Select
End Sub
```

7. Macro to Apply Special Paste Function

```
Sub SpecialPaste()
'
' SpecialPaste Macro
' Macro recorded 3/5/2006 by Richard Evans
'
' Keyboard Shortcut: Ctrl+p
'
    Selection.PasteSpecial Paste:=xlValues, Operation:=xlNone, SkipBlanks:= _
        False, Transpose:=False
End Sub
```

8. Macro to Delete Row and Move to Next Row

```
Sub DeleteLine()
'
' DeleteLine Macro
```

```
' Macro recorded 3/5/2006 by Richard Evans
'
' Keyboard Shortcut: Ctrl+k
'
    Range("A1:L53").Select
    Application.CutCopyMode = False
    Selection.Delete Shift:=xlUp
    Range("I1").Select
End Sub
```

References:

[1] B. K. P. Horn, 1977. "Understanding image intensities," Artificial Intelligence, Vol. 8, pp 201-231.

[2] B. K. P. Horn, 1979. "Hill shading and the reflectance map," Image Understanding Workshop, Palo Alto, CA.

[3] B. K. P . Horn, 1990. Height and gradient from shading. International Journal of Computer Vision, Vol. 5, No. 1.

[4] Carlotto, Mark, 1996. "Shape from Shading" web document: http://www.newfrontiersinscience.com/martianenigmas/Articles/SFS/sfs.html

[5] C. Wöhler, R. Lena, P. Lazzarotti, J. Phillips, M. Wirths, Z. Pujic, 2006. A combined spectrophotometric and morphometric study of the lunar mare dome fields near Cauchy, Arago, Hortensius, and Milichius. Icarus, article in press.

[6] R. Lena, C. Fattinnanzi, J. Phillips, C. Wöhler, 2005. A study about a dome near Yerkes; observations, measurements and classification. Selenology, vol. 25, no. 2, pp. 4-10.

DRAWINGS OF LUNAR RILLES BY J.F.JULIUS SCHMIDT

by Jim Phillips Geological Lunar Research (GLR) Group

J. F. Julius Schmidt was an indefatigable observer. He made valuable contributions in a number of fields, including observations of Jupiter, sunspots, and variable stars, however, where Schmidt truly excelled and is most remembered, was in his observations of the Moon. Schmidt's interest in the moon began at age 14 when he obtained a copy of Schröter's great work. At age 16, in 1841, he moved to Hamburg and used the telescope there regularly. He observed the moon for some 34 years, making numerous drawings and height and depth measurements. In 1858 Schmidt became director of the Athens Observatory, where he used its 6.2" refractor to continue his studies of the moon.

In 1878 Schmidt published, in 25 sections, his *Charte der Gebirge des Mondes (Map of the Mountains of the Moon)*, containing 32,856 craters (Ashbrook, 1984). Schmidt used telescopes that were of greater aperture than those used by Lohrmann and Mädler, allowing him to observe smaller details as is evident in comparing his map with those published by Lohrmann and Mädler (Whitaker, 2002). Lohrmann recorded 7,178 craters and Mädler 7,735.

While studying the lunar surface, Schmidt began recording new lunar rilles. In a letter to the British Association for the Advancement of Science dated October 6, 1865 Schmidt describes his upcoming publication, *Über Rillen auf dem Monde* (1866b), describing these rilles along with all previously discovered rilles. He included the following chart:

Between 1787 to 1801 11 rilles were discovered by Schroeter, 75 by Lohrmann between 1823 and 1827, 55 by Madler between 1832 and 1842, 6 by kinau between 1847 and 1848, and 278 by Schmidt between 1842 and 1865.

Schmidt notes that he had discovered an additional 30 or 40 rilles not included in the above chart. Regarding his publication, Schmidt (1866a) states, "I enclose only a few slight sketches of remarkable rilles, which, in case they should not yet be known to English astronomers, may give occasion to future researches." His letter also contained a drawing of the rilles east (IAU) of Mare

Serenitatis, from Posidoinius to Littrow. Schmidt's *Über Rillen auf dem Monde* (1866b) contains detailed descriptions of his drawing and a catalogue describing each of 425 rilles by lunar quadrant.

Schmidt states in his letter "I myself have never been in possession of sufficient means to produce anything important for selenography and have been obliged to content myself with small contributions…". He was a modest man indeed! I would hope that we all might make such "small contributions". Shown here are the three drawings from J. F. Julius Schmidt's *Über Rillen auf dem Monde*, and the drawing included in his letter to the BAAS.

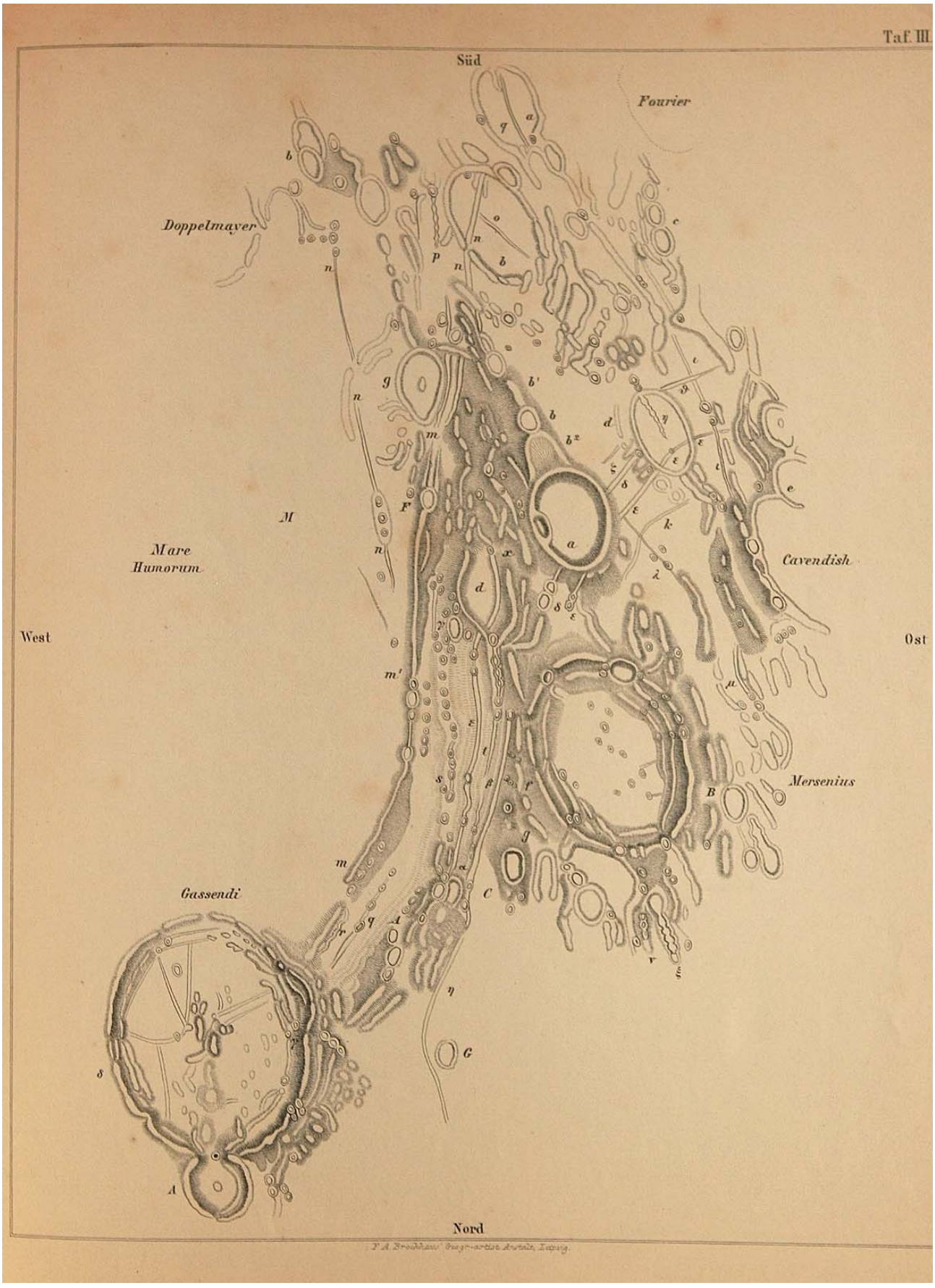
Taf. III.
Süd
Fourier
Doppelmayer
Mare
Humorum
Cavendish
West
Ost
Mersenius
Gassendi
Nord


35th Report Brit. Assoc. 1865.
(South)
Littrow
Römer
Le Monnier
MARE SERENITATIS
Posidonius
(North)

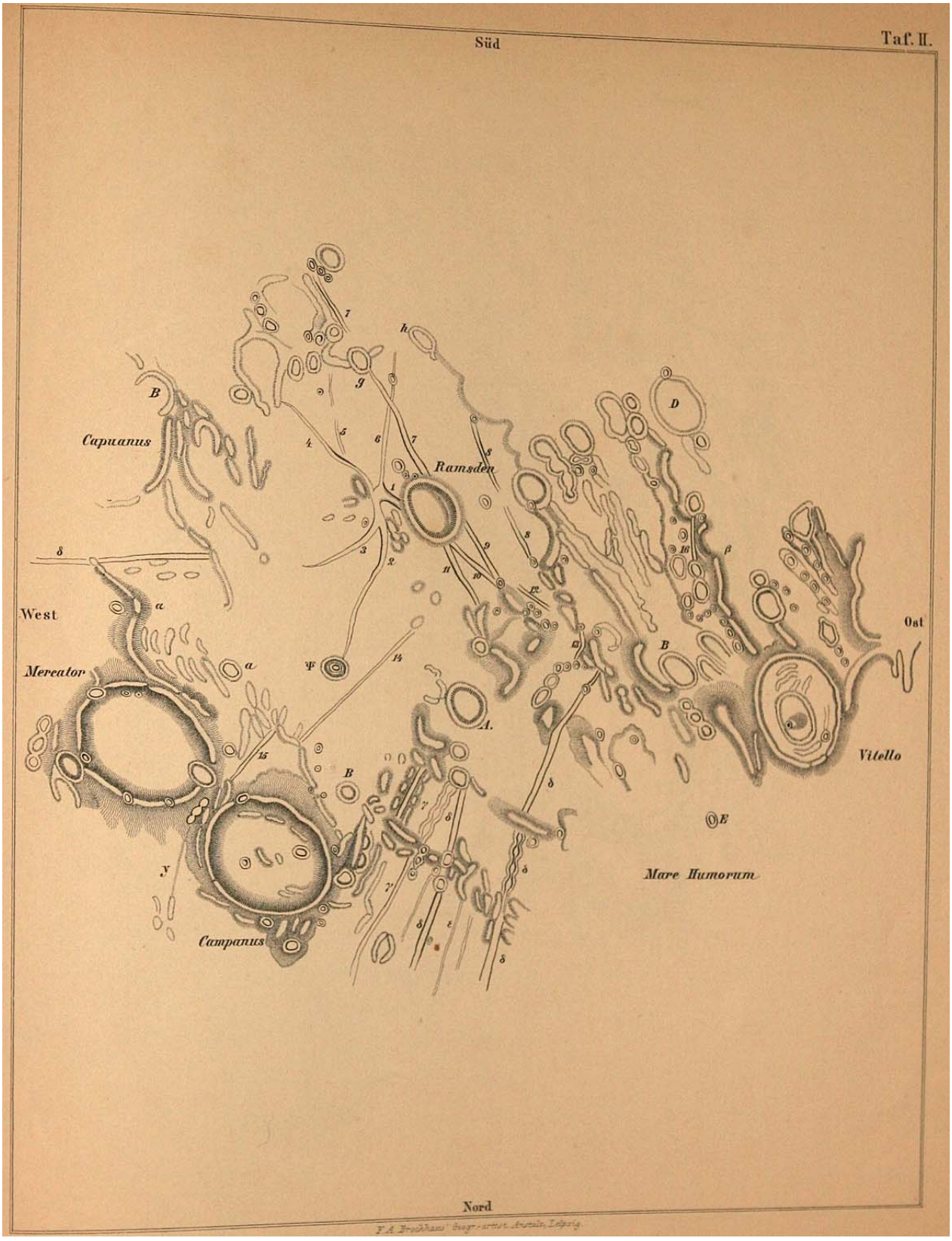
Taf. II.
Süd
Nord
West
Ost
Capuanus
Ramsden
Mercator
Campanus
Vitello
Mare Humorum

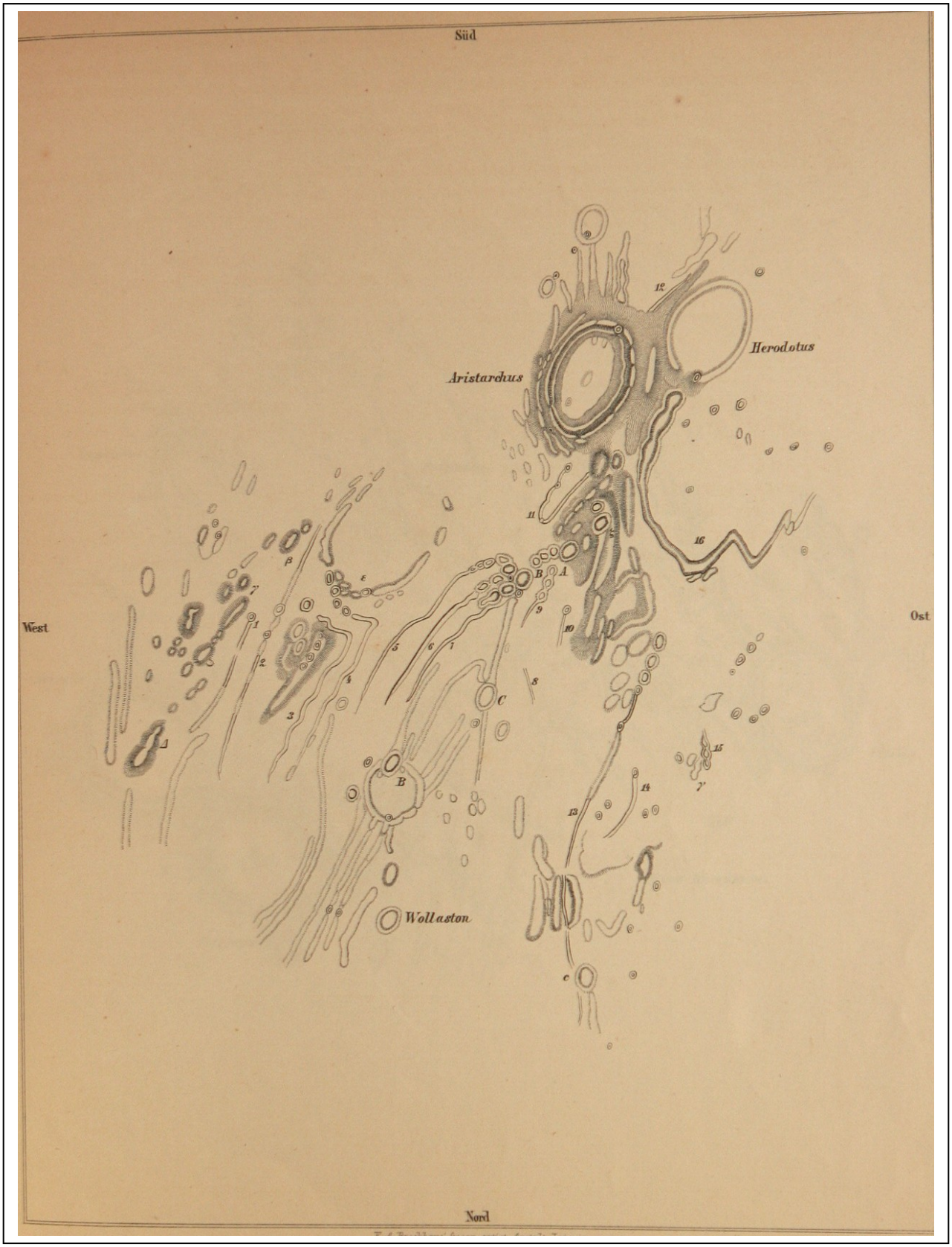
Süd
West
Ost
Nord
Aristarchus
Herodotus
Wollaston
A
B
C
D
E
α
β
γ
δ
ε
1
2
3
4
5
6
7
8
9
10
11
12
13
14
15
16

References

Ashbrook, Joseph (1984) *The Astronomical Scrapbook – Skywatchers, Pioneers and Seekers in Astronomy*. Cambridge University Press, p 251–258.

Schmidt, J.F.J. (1866a) *Report of the Thirty-Fifth Meeting of the British Association for the Advancement of Science*; held at Birmingham in September 1866. P. 305–307.

Schmidt, J.F.J. (1866b) *Über Rillen auf dem Monde*. Leipzig, Plates I–IV

Whitaker, E.A. (2002) *Mapping and Naming the Moon*. Cambridge University Press, pp 242.

SELENOLOGY TODAY
GUIDE FOR AUTHORS

1. GENERAL INFORMATION

1.1 Overview

Selenology Today is devoted to the publication of contributions in the field of lunar studies. Manuscripts reporting the results of new research concerning the astronomy, geology, physics, chemistry, and other scientific aspects of Earth's Moon are welcome. ***Selenology Today*** publishes papers devoted exclusively to the Moon. Reviews, historical papers, and manuscripts describing observing or spacecraft instrumentation are considered.

The language of ***Selenology Today*** is English. Authors whose first language is not English should have their manuscripts reviewed by an English-speaking colleague to refine use of the English language (vocabulary, grammar, syntax). At the discretion of ***Selenology Today***, manuscripts may be returned for English language corrections.

All papers are reviewed by independent reviewers. The identities and affiliations of authors are not provided to reviewers, nor are reviewers' names disclosed to authors. The goal is to complete reviews within 30 days of receipt of a manuscript by the Editor. Authors will usually be asked to respond to criticisms and suggestions by the reviewers prior to publication. Reviewers may be consulted at the Editor's discretion about resubmitted manuscripts. Manuscripts accepted for publication will be returned to the author(s) for final editing before being placed in the queue for publication. Manuscripts not accepted will either be (1) rejected or (2) returned to the author(s) for revision and subsequent reconsideration by the reviewers. Authors who do not revise and return a "to-be-reconsidered" manuscript within 90 days from receipt

of reviews may have their manuscript withdrawn from the review process.

Manuscripts are accepted for review with the understanding that the same work has not been published and that its submission for publication has been approved by all of the authors.

Articles and any other material published in *Selenology Today* represent the opinions of the authors and should not be construed to reflect the opinions of *Selenology Today*.

There are no page charges.

1.2 Manuscripts

Electronic Submission

The *Selenology Today* Editorial Office prefers the electronic submission of manuscripts via e-mail selenology_today@christian-woehler.de

Selenology Today will accept *Microsoft Word* or .pdf files. Figures will be accepted in JPG formats only at 300 dpi for halftones and 1200 dpi for line art.

Authors should retain an original copy of their manuscript. At least one set of figures should be of high quality and suitable for direct photographic reproduction. All manuscripts must be printed or typed with wide margins and double-spaced throughout, including references and footnotes. Number each page of the manuscript. Include on the first page the title of the paper and the names(s) and affiliation(s) of the author(s). At the bottom of the first page note the number of manuscript pages, figures, and tables.

Present results logically. Take special care in composing the title and abstract, since these will be the most frequently read sections of the paper. In the title, specific words are preferable to general ones. The abstract should summarize the conclusions of the research, including quantitative results where appropriate, rather than merely stating the problem.

Whenever possible, quotients in mathematical expressions should employ the solidus (/) rather than being displayed in built-up form. However, for units, exponential notation is preferred (e.g., erg cm^{-2} s^{-1}, not erg/cm^2s).

1.3 Format Requirements

Manuscripts submitted for peer review must be prepared as outlined below. Manuscripts that do not conform to the requirements described below will be returned for format revisions before they are sent for review.

Typing: Manuscripts must be double-spaced. An 11 or 12-point font such as Times New Roman or Arial is preferred. When prepared on paper, authors should use one side of 8½- by 11-inch or A4 International (210- by 297-mm) white paper, with 30-mm (1¼-inch) margins all around. For review purposes every part of the manuscript must be double-spaced, including title page, abstract, text, footnotes references, appendices, and figure captions.

Title Page: Authors should strive for titles no longer than eight to ten words. The title page shall include a short title and a one-sentence description of the paper's content to accompany the title in the ***Selenology Today*** Table of Contents. To facilitate the blind review process, authors' names, affiliations, and addresses should be provided only on a cover letter, not on the title page. Authors should indicate both their current affiliation (if applicable) and, if different, their affiliation (if applicable) at the time the research was performed.

Abstract: All manuscripts submitted for peer review (except "Briefs," i.e., manuscripts of fewer than 5 typewritten pages) must include an abstract of 150 words or less. The abstract should be stand-alone and understandable without reference to the text.

1.4 Figures and Tables

When described in the body of the text, a table should be referred to as Table X, an equation as Eq. Y, and a figure as Fig. Z (use these abbreviations everywhere except at the beginning of a sentence).

Tables are numbered consecutively with Arabic numerals in order of their citation in the text. Each table should be typed, *single-spaced*, with due regard to the proportions of the printed page. All tables should bear appropriate headings.

Metric System: The metric system (SI Units) will be employed throughout a manuscript except in cases where the English System has special merit stemming from accepted conventional usage (e.g., 9- by 9-inch photograph, 6-inch focal length).

Equations: Authors should express equations as simply as possible. They should include only those equations required by an average reader to understand the technical arguments in the manuscript. Manuscripts that appear to have excessive mathematical notation may be returned to the author for revision. Whenever possible, authors are encouraged to use the **Insert** and **Symbol** capabilities of *Microsoft Word* to build simple equations. If that is not possible, the author must

indicate in the letter of transmittal which software was used to create the equations. *Microsoft Equation, Microsoft Equation Editor*, or *MathType format* should be used only if absolutely necessary. Equations must be numbered and should be embedded in the text file.

1.5 Literature Citations

Literature citations ***in the text*** should be in one of the following forms: Estrada and Cuzzi 1996 (for two authors); Zappalà *et al*. 1995 (for three or more authors); Ip 1995, p. 299 (for reference to a specific page). To distinguish two or more works by the same author(s) in the same year, use suffices a, b, etc., following the year (e.g., Encrenaz *et al.* 1996a, 1996b).

References to personal communications, manuscripts in preparation, unpublished work, anonymous ftp files, or databases should not be included in the bibliography, but should be cited parenthetically in the text.

Literature citations ***in the bibliography*** should be listed alphabetically (and then chronologically) according to the surname of the (first) author. The listings of authors having multiple entries should first list all papers by the author alone chronologically, then two author papers, alphabetically and then chronologically, and finally all multiple author papers. This latter group should be listed alphabetically according to the surname of the (first) author and then chronologically. Journal references should contain the names and initials of all authors, the year, the title of the article, and the standard abbreviation of the journal, the volume number, and the first and last pages. As an exception to this rule, any article with more than 10 co-authors may be listed using a style like "Belton, M.J.S., and 10 colleagues,..." Shown below are examples of the proper reference forms for a book, a journal article, and a book chapter, respectively.

Format for references in the reference list will be as follows:

Books:
Price, F.W., 1988. *The Moon Observer's Handbook*, Cambridge University Press, UK, 309 p.

Articles (or Chapters) in a Book:
Hapke, B., 1971. Optical Properties of the Lunar Surface, *Physics and Astronomy of the Moon* (Z. Kopal, editor), Academic Press, New York, N.Y., pp. 155-211.

Journal Articles:
Bell, J.F. and Hapke, B.R., 1984. Lunar Dark-Haloed Impact Craters: Origin and Implications for Early Mare Volcanism, *Journal of Geophysical Research,* 89(B8):6899-6910.

Proceedings (printed):
Burley, J.M., and B.M. Middlehurst,1966. Apparent Lunar Activity, *Proceedings of the National Academy of Sciences*, p1007.

Proceedings (CD-ROM):
Burley, J.M., and B.M. Middlehurst,1966. Apparent Lunar Activity, *Proceedings of the National Academy of Sciences*, p1007, unpaginated CD-ROM.

Thesis and Dissertations:
Puskar, R. J., 1983. *The Opposition Effect in Optical Scattering from Rough Surfaces*, Ph.D. dissertation, The Ohio State University Journal, Columbus, OH, 336 p.

Website References:
Kapral, C.A. and Garfinkle, R.A., 2005. GLR Lunar Domes Catalog, URL: http://www.glrgroup.org/domes.htm, (last date accessed: 15 August 2005).

1.6 Notes

Short papers on especially topical subjects will be given unusually rapid handling if they satisfy the following limitations on length:

• Notes should be typed double-spaced and should be no longer than ten (10) pages, including a very brief abstract of one or two sentences.

Our goal is that ***Selenology Today*** will publish Notes within 30 days of submission, if no revision is required. We will try to complete reviewing and editorial handling in less than one month.

1.7 Preparation of Supplemental Material

Selenology Today accepts electronic supplementary material to support and enhance your scientific research. Supplementary files offer additional possibilities for publishing supporting applications, movies, animation sequences, high-resolution images, background datasets, sound clips, and more. Supplementary files supplied will be published online alongside the electronic version of your article. To ensure that your submitted material is directly usable, please provide the data in one of our recommended file formats. Authors should submit the material in electronic format together with the article and supply a concise and descriptive caption for each file.

1.8 Proofs

Selenology Today will do everything possible to get your article corrected and published as quickly and accurately as possible. Therefore, it is important that all of your corrections are sent back to us in one communication from the corresponding author. Subsequent corrections will not be possible, so please ensure your first sending is complete.

2. ELECTRONIC SUBMISSION OF MANUSCRIPTS

2.1 Overview

Selenology Today accepts new and revised manuscripts electronically. All submitted and revised manuscripts are handled through our Web site, with password-protected access granted to authors and reviewers only. Please note that manuscripts submitted in hardcopy format will be scanned for incorporation into our Web-based system in PDF format, so authors are strongly encouraged to submit electronically to maintain the maximum fidelity of their images and text.

2.2 Acknowledgments

In keeping with the process of blind reviews, authors are asked not to include acknowledgments in manuscripts submitted for peer review. An acknowledgment may reveal a considerable amount of information for reviewers that is not necessary or desirable for their evaluation of the manuscript. After a manuscript is accepted for publication, the lead author will be encouraged to insert appropriate acknowledgments.